Library of Congress Cataloging-in-Publication Data
Smart, Lesley. Solid state chemistry: an introduction/Lesley Smart and Elaine Moore.–3rd ed. p. cm. Includes bibliographical references and index. ISBN 0-7487-7516-1 (alk. paper) 1. Solid state chemistry. I. Moore, Elaine (Elaine A.) II. Title. QD478.S53 2005 541′.0421–dc22 2004058533

T&F informa

Taylor & Francis Group is the Academic Division of T&F Informa plc.
Visit the Taylor & Francis Web site at http://www.taylorandfrancis.com
and the CRC Press Web site at http://www.crcpress.com

Dedicated to

Graham, Sam, Rosemary, and Laura

gamma	Γ	γ	omicron	O	o
delta	Δ	δ	pi	Π	π
epsilon	E	ε	rho	P	ρ
zeta	Z	ζ	sigma	∑	σ
eta	H	η	tau	T	τ
theta	Θ	θ	upsilon	Y	υ
iota	I	ι	phi	Φ	φ
kappa	K	κ	chi	X	χ
lambda	Λ	λ	psi	Ψ	ψ
mu	M	μ	omega	Ω	ω

PERIODIC CLASSIFICATION OF THE ELEMENTS

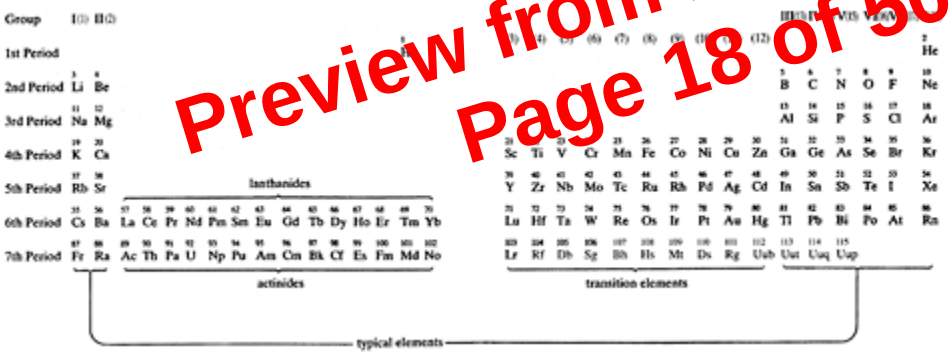

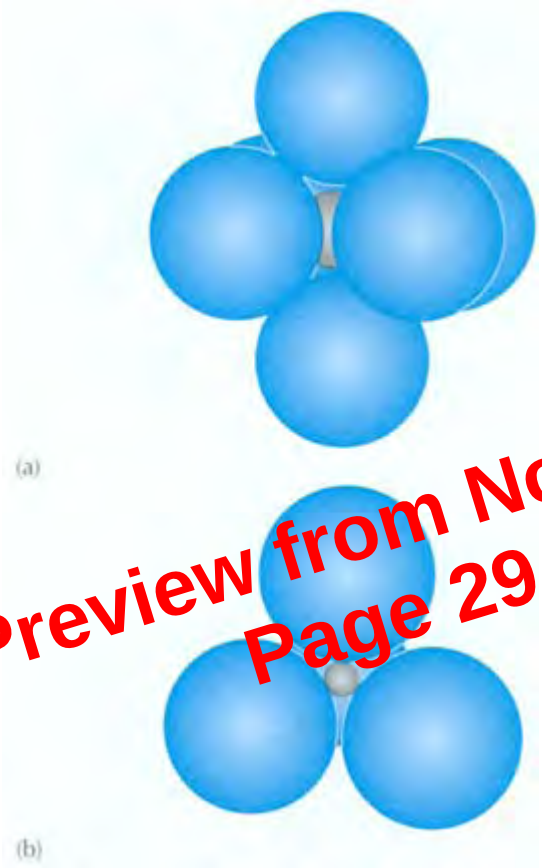

FIGURE 1.7 (a) A sphere of radius 0.414*r* fitting into an octahedral hole; (b) a sphere of radius 0.225*r* fitting into a tetrahedral hole.

1.3 BODY-CENTRED AND PRIMITIVE STRUCTURES

Some metals do not adopt a close-packed structure but have a slightly less efficient packing method: this is the **body-centred cubic structure *(bcc),*** shown in Figure 1.8. (Unlike the previous diagrams, the positions of the atoms are now represented here—and in subsequent diagrams—by small spheres which do not touch: this is merely a device to open up the structure and allow it to be seen more clearly—the whole question of atom and ion size is discussed in Section 1.6.4.) In this structure an atom in the middle of a cube is surrounded by *eight identical and equidistant* atoms at the corners of the cube—

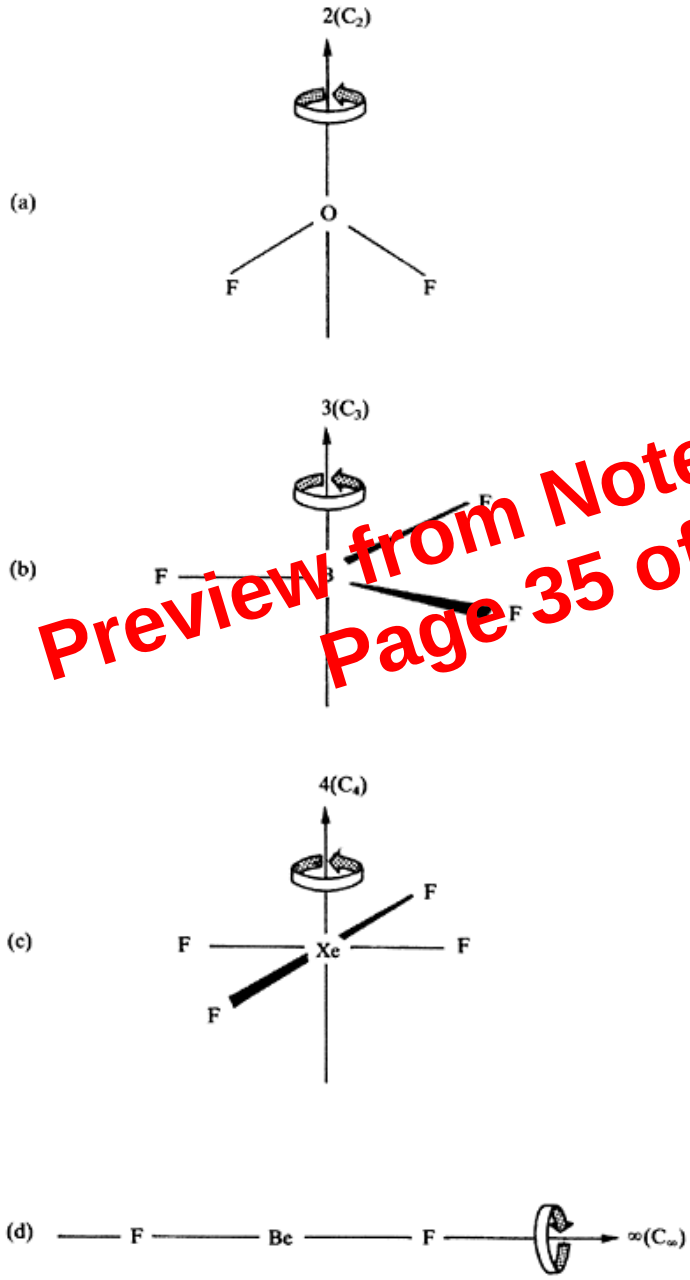

FIGURE 1.12 Axes of symmetry in molecules: (a) twofold axis in OF_2, (b)

are the basic building blocks of the crystals, they must be space-filling (i.e., they must pack together to fill all space). All the possible unit cell shapes that can fulfill this criterion are illustrated in Figure 1.23 and their specifications are listed in Table 1.2.These are known as the **seven crystal systems** or **classes**.These unit cell shapes are determined by minimum symmetry requirements which are also detailed in Table 1.2.

The three-dimensional unit cell includes *four* different types (see Figure 1.24):

1. The **primitive** unit cell—symbol **P**—has a lattice point at each corner.
2. The **body-centred** unit cell—symbol **I**—has a lattice point at each corner and one at the centre of the cell.
3. The **face-centred** unit cell—symbol **F**—has a lattice point at each corner and one in the centre of each face.
4. The **face-centred** unit cell—symbol **A, B,** or **C**—has a lattice point at each corner, and one in the centres of one pair of opposite faces (e.g., an A-centred cell has lattice points in the centres of the *bc* faces).

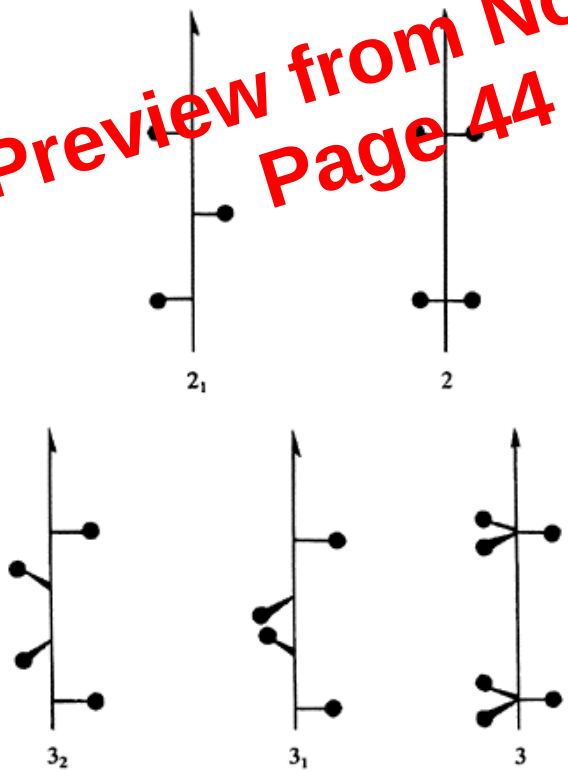

FIGURE 1.21 Comparison of the effects of twofold and threefold rotation axes and screw axes.

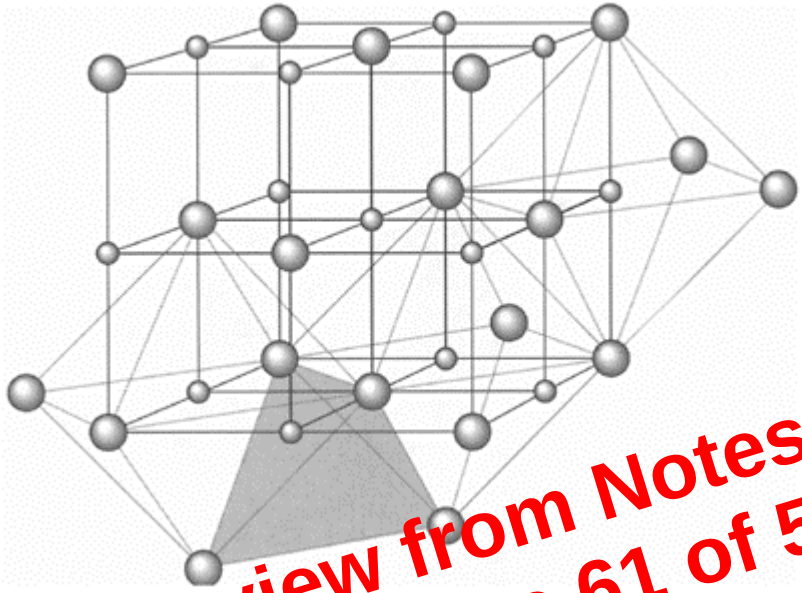

FIGURE 1.35 NaCl structure showing edge-sharing of octahedra and the enclosed tetrahedral space (shaded).

linking of octahedra by different methods effectively eliminates atoms because some of the atoms are now shared between them: two MO_6 octahedra linked through a vertex has the formula, M_2O_{11}; two MO_6 octahedra linked through an edge has the formula, M_2O_{10}; two MO_6 octahedra linked through a face has the formula, M_2O_9.

The NaCl structure can be described in terms of $NaCl_6$ octahedra sharing edges. An octahedron has 12 edges, and each one is shared by two octahedra in the NaCl structure. This is illustrated in Figure 1.35, which shows a NaCl unit cell with three $NaCl_6$ octahedra shown in outline, and one of the resulting tetrahedral spaces is depicted by shading.

The Nickel Arsenide Structure (NiAs)

The nickel arsenide structure is the equivalent of the sodium chloride structure in hexagonal close-packing. It can be described as an *hcp* array of arsenic atoms with nickel atoms occupying the octahedral holes. The geometry about the nickel atoms is thus octahedral. This is not the case for arsenic: each arsenic atom sits in the centre of a **trigonal prism** of six nickel atoms (Figure 1.36).

octahedral sites. Examples of inverse-spinels include magnetite, Fe_3O_4, (see Chapter 9, Section 9.7) $Fe(MgFe)O_4$, and $Fe(ZnFe)O_4$.

The Perovskite Structure

This structure is named after the mineral $CaTiO_3$. A unit cell is shown in Figure 1.44(a): This unit cell is known as the A-type because if we take the general formula ABX_3 for the perovskites, then theA atom is at the centre in this cell. The central Ca (A) atom is coordinated to 8 Ti atoms (B) at the corners and to 12 oxygens (X) at the midpoints of the cell edges. The structure can be usefully described in other ways. First, it can be described as a *ccp* array of A and X atoms with the B atoms occupying the octahedral holes (compare with the unit cell of NaCl in Figure 1.31 if you want to check this). Second, perovskite has the same octahedral framework as ReO_3 based on BX_6 octahedra with an A atom added in at the centre of the cell (Figure 1.42(b)). Compounds adopting this structure include $SrTiO_3$, $SrZrO_3$, $SrHfO_3$, $SrSnO_3$, and $BaSnO_3$. The structures of the high temperature superconductors are based on this structure (see Chapter 10, Section 10.3.1).

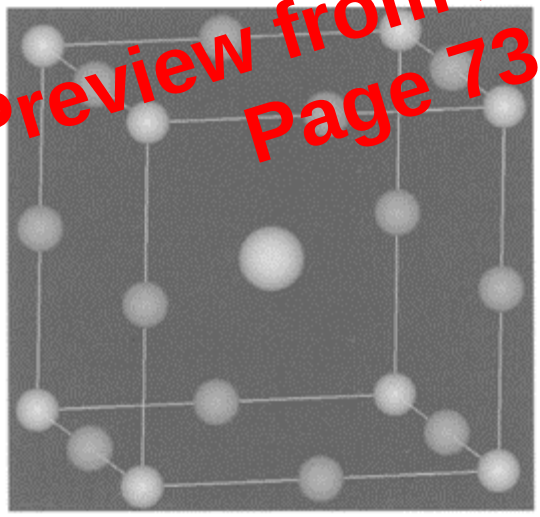

FIGURE 1.44 The perovskite structure of compounds ABX_3, such as $CaTiO_3$. See colour insert following page 196. Ca, green sphere; Ti, silver spheres; O, red spheres.

The Ilmenite Structure

The ilmenite structure is adopted by oxides of formula ABO_3 when A and B are similar in size and their total charge adds up to +6. The structure is named after the mineral of $Fe^{II}Ti^{IV}O3$, and the structure is very similar to the corundum structure described

		alternate pairs of layers have two-thirds of the octahedral sites occupied		VCl_3
M_2X_3	6:4	Two-thirds octahedral		Corundum: α-Al_2O_3, α-Fe_2O_3, V_2O_3, Ti_2O_3, α-Cr_2O_3
ABO_3		Two-thirds octahedral		Ilmenite: $FeTiO_3$
AB_2O_4		One-eighth tetrahedral and one-half octahedral	Spinel: $MgAl_2O_4$ inverse spinel: $MgFe_2O_4$, Fe_3O_4	Olivine: Mg_2SiO_4

size is going to be affected by their environment. Nevertheless, it is a useful concept to develop a bit further as it enables us to describe some of the ionic crystal structures in a simple pictorial way.

There have been many suggestions as to how individual ionic radii can be assigned, and the literature contains several different sets of values. Each set is named after the person(s) who originated the method of determining the radii. We will describe some of these methods briefly before listing the values most commonly used at present. It is most important to remember that you must not mix radii from more than one set of values. Even though the values vary considerably from set to set, each set is internally consistent (i.e., if you add together two radii from one set

TABLE 1.8 Interatomic distances of some alkali halides, $r_{M\text{-}x}$/pm

	F^-		Cl^-		Br^-		I^-
Li^+	201	**56**	257	**18**	275	**27**	302
	30		**24**		**23**		**21**
Na^+	231	**50**	281	**17**	298	**25**	323
	35		**33**		**31**		**30**
K^+	266	**48**	314	**15**	329	**24**	353
	16		**14**		**14**		**13**
Rb^+	282	**46**	328	**15**	343	**23**	366

of values, you will obtain an approximately correct internuclear distance as determined from the crystal structure).

The internuclear distances can be determined by X-ray crystallography. In order to obtain values for individual ionic radii from these, the value of one radius needs to be fixed by some method. Originally in 1920, Landé suggested that in the alkali halide with

simplistic—ions are not hard spheres, but are polarized under the influence of other ions instead. In larger ions, the valence electrons are further away from the nucleus, and shielded from its influence by the inner core electrons, and so the electron cloud is more easily distorted. The ability of an ion to distort an electron cloud—its polarizing power—is greater for small ions with high charge; the distortion of the electron cloud means that the bonding between two such ions becomes more directional in character. This means that the bonding involved is rarely truly ionic but frequently involves at least some degree of covalency. The higher the formal charge on a metal ion, the greater will be the proportion of covalent

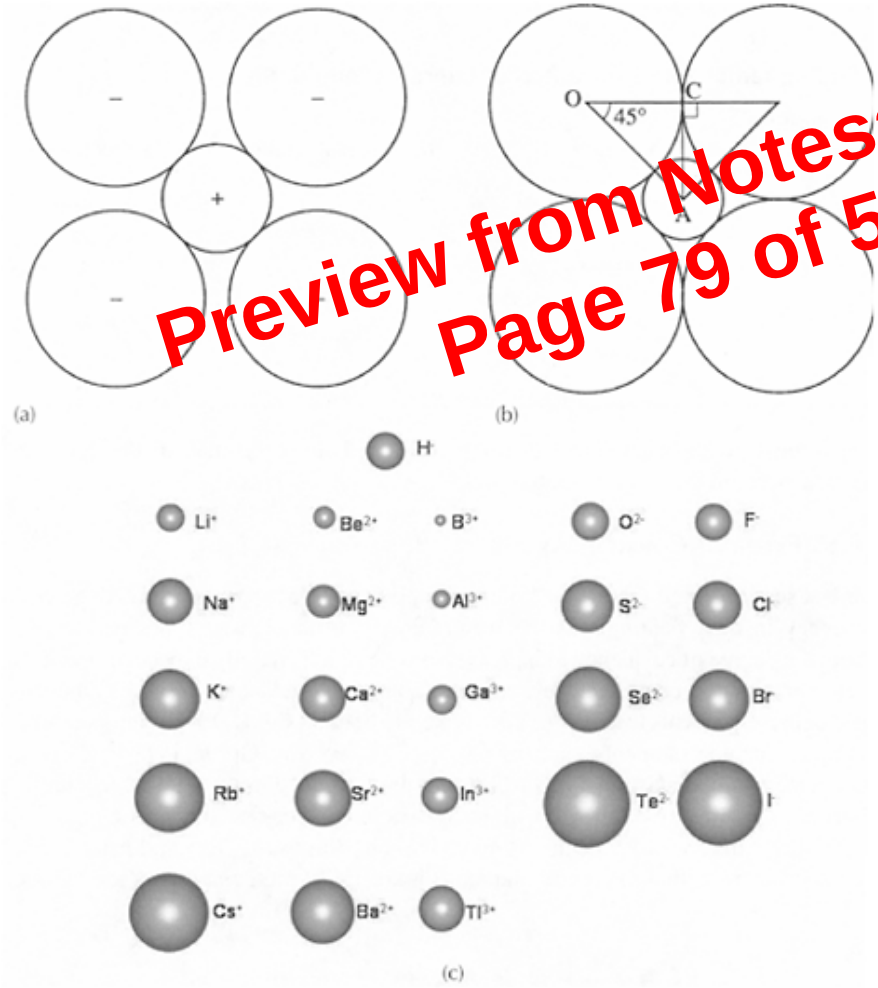

FIGURE 1.46 (a) Anions packed around a cation on a horizontal plane, (b) anion-anion contact on a horizontal

For our final example in this section, we will look at the structure of another polymorph of carbon. Normal **graphite** is illustrated in Figure 1.49. (There are other

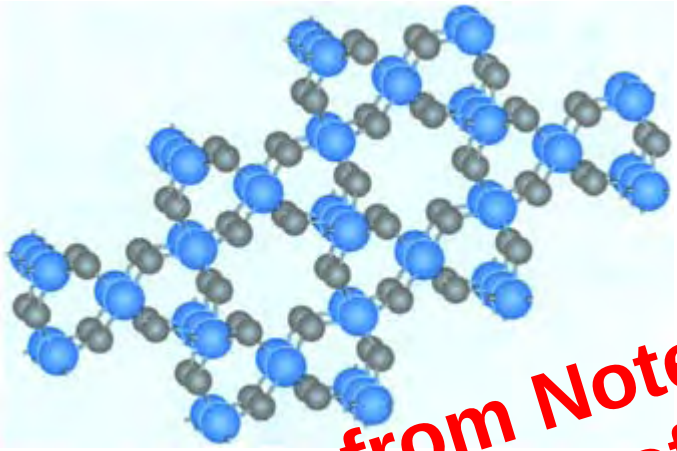

FIGURE 1.48 The β-quartz structure.

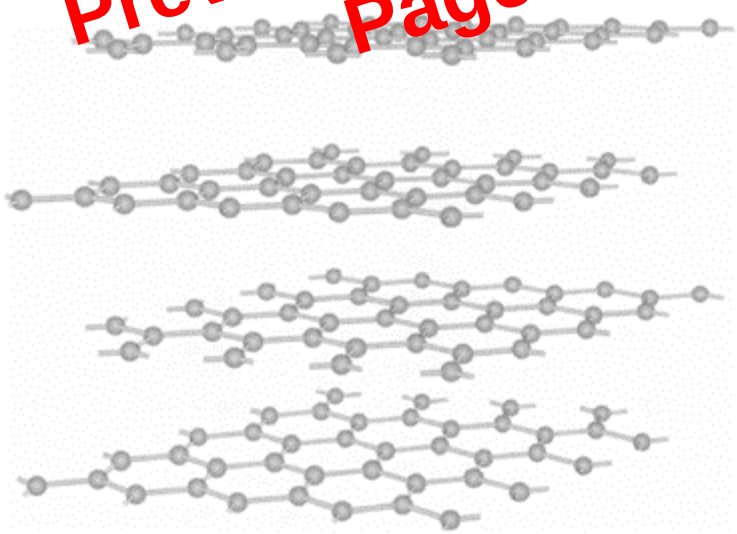

FIGURE 1.49 SThe crystal structure of graphite.

graphite structures that are more complex.) The structure of normal graphite consists of two-dimensional layers of carbon atoms joined together in a hexagonal array. Within the layers, each carbon atom is strongly bonded to three others at a distance of 142 pm. This carbon-carbon distance is rather shorter than the one observed in diamond, due to the

pack together in regular arrays in ionic crystals, in such a way as to maximize Coulombic attraction, and minimize repulsions.

Covalent Bonding

In covalent bonds, the electrons are shared between two atoms resulting in a buildup of electron density between the atoms. Covalent bonds are strong and directional.

Charge-Dipole and Dipole-Dipole Interactions

In a covalent bond, electronegative elements such as oxygen and nitrogen attract an unequal share of the bonding electrons, such that one end of the bond acquires a partial negative charge, δ−, and the other end a partial positive charge, δ+. The separation of negative and positive charge creates an **electric dipole,** and the molecule can align itself in an electric field. Such molecules are said to be **polar**. The partial electronic charges on polar molecules can attract one another in a **dipole-dipole interaction**. The dipole-dipole interaction is about 100 times weaker than ionic interactions and falls off quickly with distance, as a function of $\frac{1}{r^3}$.

Polar molecules can also interact with ions in a **charge-dipole interaction** which is about 10 to 20 times weaker than ion-ion interactions, and which decreases with distance as $\frac{1}{r^2}$.

London Dispersion Forces

Even if molecules do not possess a permanent dipole moment weak forces can exist between them. The movement of the valence electrons creates ‘transient dipoles’, and these in turn induce dipole moments in adjacent molecules. The transient dipole in one molecule can be attracted to the transient dipole in a neighbouring molecule, and the result is a weak, short-range attractive force known as the **London dispersion force**. These dispersion forces drop off rapidly with distance, decreasing as a function of $\frac{1}{r^6}$.

The weak nonbonded interactions that occur between molecules are often referred to collectively as **van der Waals forces**.

Hydrogen-Bonding

In one special case, polar interactions are strong enough for them to be exceptionally important in dictating the structure of the solid and liquid phases. Where hydrogen is bonded to a very electronegative element such as oxygen or fluorine, there is a partial negative charge, δ−, on the electronegative element, and an equal and opposite δ+ charge on the hydrogen. The positively charged $H^{\delta+}$ can also be attracted to the partial negative charge on a neighbouring molecule, forming a weak bond known as a **hydrogen-bond,** O–H---O, and pulling the three atoms almost into a straight line. A network of alternating

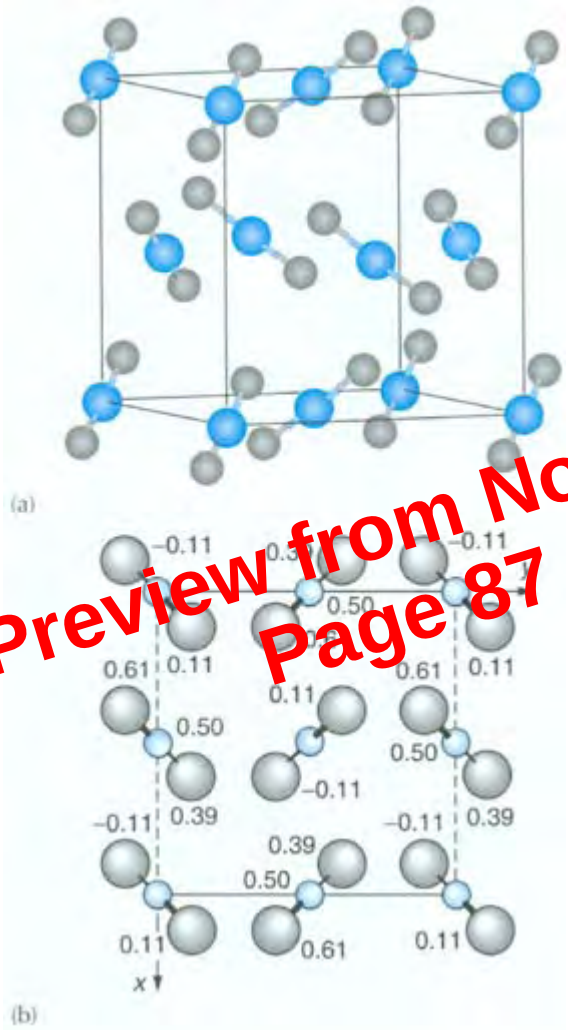

FIGURE 1.50 (a) The crystal structure of CO_2, (b) packing diagram of the unit cell of CO_2 projected on to the *xy* plane. The heights of the atoms are expressed as fractional coordinates of c. C, blue spheres; O, grey spheres.

this only gives a broad overview, and is intended as a guide only: not every crystal will fall exactly into one of these categories.

$$E = -\frac{e^2}{4\pi\varepsilon_0 r} \tag{1.6}$$

and where the *magnitudes* of the charges on the ions are Z_+ and Z_-, for the cation and anion, respectively, by

$$E = -\frac{Z_+ Z_- e^2}{4\pi\varepsilon_0 r} \tag{1.7}$$

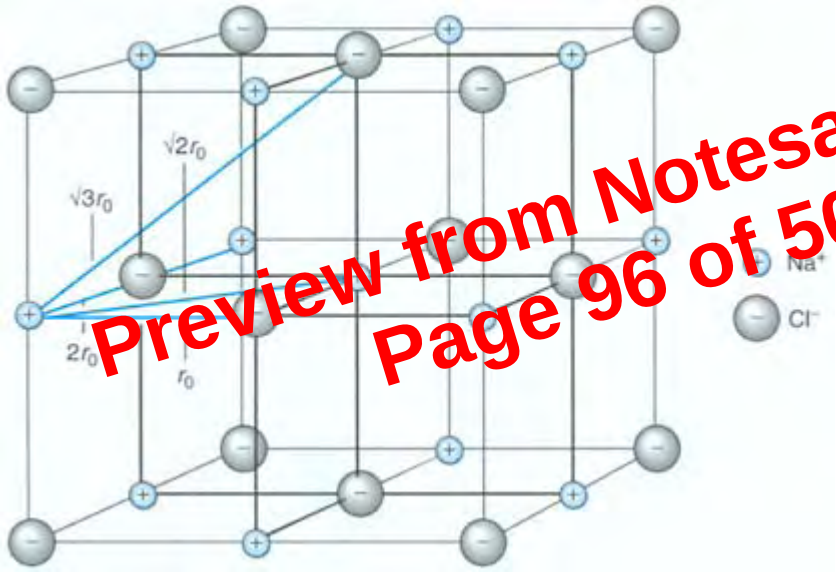

FIGURE 1.57 Sodium chloride structure showing internuclear distances.

(e is the electronic charge, 1.6×10^{-19} C, and ε_0 is the permittivity of a vacuum, 8.854×10^{-12} F m^{-1}).

The energy due to coulombic interactions in a crystal is calculated for a particular structure by summing all the ion-pair interactions, thus producing an infinite series. The series will include terms due to the attraction of the opposite charges on cations and anions and repulsion terms due to cation/cation and anion/anion interactions. Figure 1.57 depicts some of these interactions for the NaCl structure. The Na^+ ion in the centre is immediately surrounded by 6 Cl^- ions at a distance of r, then by 12 cations at a distance of $\sqrt{2}\,r$, then by eight anions at $\sqrt{3}\,r$, followed by a further 6 cations at $2r$, and so on. The coulombic energy of interaction is given by the summation of all these interactions:

$\Delta H_f^{\ominus}$ (NaCl,s)	−411		
L(MCl,s)			

2.4.2 SOLVING SINGLE CRYSTAL STRUCTURES

It would seem to be an unresolvable problem—to calculate the structure factors we need the atomic positions and to find the atomic positions we need both the amplitude and the phase of the resultant waves, and we only have the amplitude. Fortunately, many scientists over the years have worked at finding ways around this problem, and have been extremely successful, to the extent that for many systems the solving of the structure has become a routine and fast procedure.

Single crystal X-ray diffraction data is nowadays collected using a computer controlled diffractometer, which measures the Bragg angle θ and the intensity I for each *hkl* reflection. Many modern diffractometers employ a flat-plate detector (CCD), so that all the reflections can be collected and measured at the same time. A full data set, which can be thousands of reflections, can be accumulated in hours rather than the days or weeks of earlier times.

To summarize what we know about a structure:

- The size and shape of the unit cell is determined, usually from rotation photographs and scanning routines directly on the diffractometer.
- The reflections are indexed, and from the systematic absences the Bravais lattice and the translational symmetry elements of the structure determined; this information often determines the space group unequivocally, or narrows the possibilities down to a choice of two or three.
- The intensities of the indexed reflections are measured and stored as a data file.
- Correction factors are applied to the raw intensity data.
- Finally, the square roots of the corrected data are taken to give a set of observed structure factors. These are known as $\boldsymbol{F}_{\mathbf{obs}}$ or $\boldsymbol{F}_{\mathbf{o}}$.
- To calculate the electron density distribution in the unit cell, we need to know not only the magnitudes of the structure factors, but also their phase.

Crystal structures are solved by creating a set of trial phases for the structure factors. Two main methods are used to do this. The first is known as the **Patterson** method, and it relies on the presence of at least one (but not many) heavy atoms in the unit cell and so is useful for solving many inorganic molecular structures. The second is called **direct methods,** and it is best used for structures where the atoms have similar scattering properties. Direct methods calculate mathematical probabilities for the phase values and hence an electron density map of the unit cell; theoreticians have produced packages of accessible computer programs for solving and refining structures.

Once the atoms in a structure have been located, a calculated set of structure factors, $\boldsymbol{F}_{\mathbf{calc}}$ or $\boldsymbol{F}_{\mathbf{c}}$ is determined for comparison with the $\boldsymbol{F}_{\mathrm{obs}}$ magnitudes, and the positions of the atoms are refined using **least-squares methods,** for which standard computer programs are available. In practice, atoms vibrate about their equilibrium positions; this is often called **thermal motion,** although it depends not only on the temperature, but also on the mass of the atom and the strengths of the bonds holding it. The higher the temperature, the bigger the amplitude of vibration and the electron density becomes spread out over a larger volume, thus causing the scattering power of the atom to fall off more quickly. Part of the refinement procedure is to allow the electron density of each atom to refine in a sphere around the nucleus. Structure determinations usually quote an adjustable parameter known as the **isotropic displacement parameter, *B*** (also called the

C; (b) analysis of the metal particle sizes of this catalyst.

absorption and other effects, to give both qualitative and quantitative analysis of the elements present (for elements of atomic number greater than 11) in the irradiated particle, a technique known as **energy dispersive analysis of X-rays (EDAX or EDX)** (Figure 2.18).

FIGURE 2.17 HREM image showing the atomic sites on the *111* plane of a Si crystal. (Courtesy of Dipl.-Ing. Michael Stöger-Pollach, Vienna University of Technology.)

2.7 X-RAY ABSORPTION SPECTROSCOPY

2.7.1 EXTENDED X-RAY ABSORPTION FINE STRUCTURE (EXAFS)

In high energy accelerators, electrons are injected into an electron storage ring (approximately 30 m in diameter) captured, and accelerated around this circular path by a

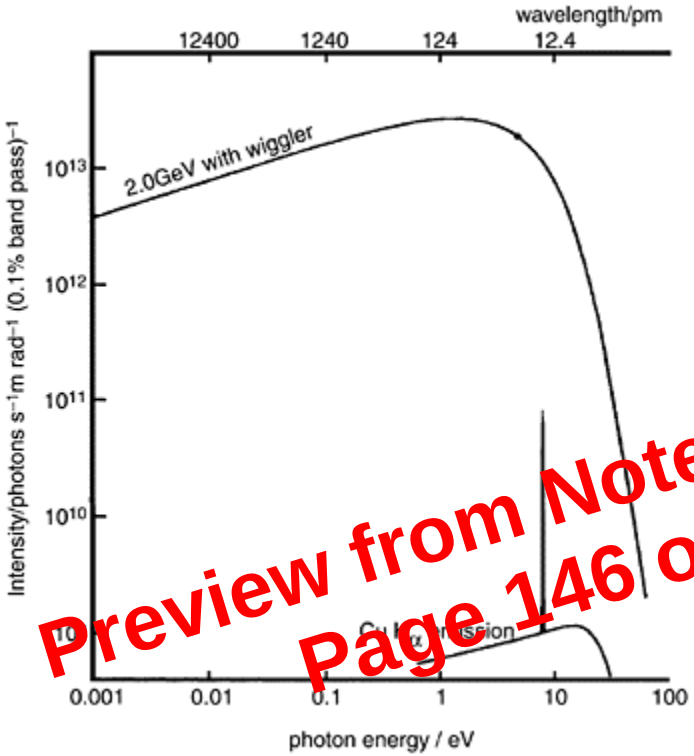

FIGURE 2.20 Synchrotron radiation profile at 2 GeV compared with Cu K_α emission.

single plane of a carefully cut crystal such as Si *(220);* often, two crystals are used, as illustrated in the schematic diagram of a double crystal monochromator in Figure 2.22. By changing the Bragg angle of reflection, the frequency of the X-rays selected may be changed, and thus the absorption edges of a wide range of elements can be studied.

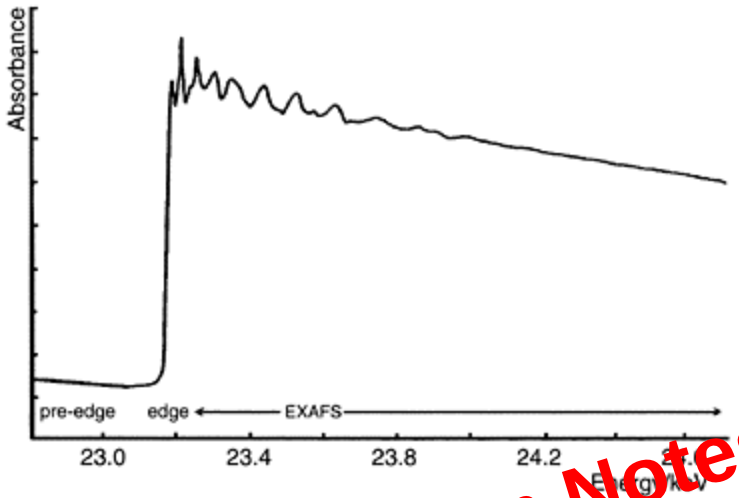

FIGURE 2.21 The Pt absorption edge and EXAFS.

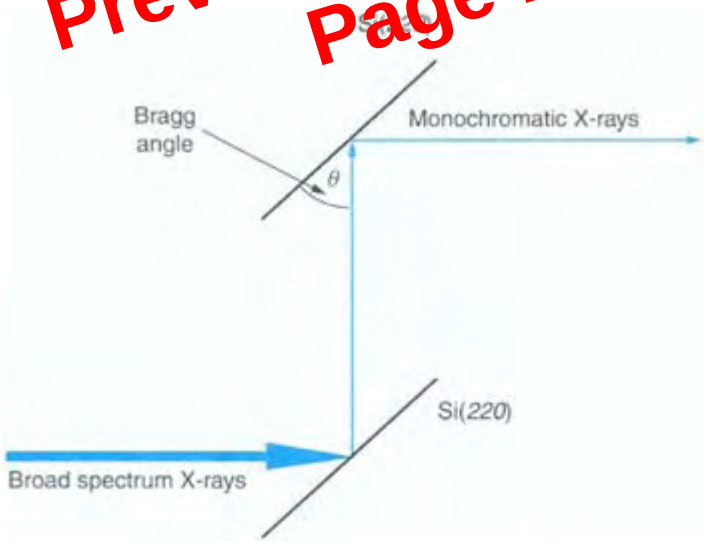

FIGURE 2.22 Bragg reflections from a double-crystal monochromator. From the Bragg equation, $n\lambda=2d\sin\theta$, d for the planes of the crystal stays constant, so changing the angle changes the wavelength of the X-rays reflected.

Two crystals are used to make the exit beam parallel to the entrance beam. Curved crystals focus the X-rays.

The waves of the ejected photoelectron from the **K** shell can be thought of as a spherical wave emanating from the nucleus of the absorbing atom; this encounters neighbouring atoms and is partially scattered by them producing a phase shift (Figure 2.23). Depending on the phase shift experienced by the electron, the reflected waves can then interfere constructively or destructively with the outgoing wave, producing a net interference pattern at the nucleus of the original atom. Absorption by the original atom is now modified, and the effect is seen as sinusoidal oscillations or **fine structure** superimposed on the absorption edge (Figure 2.21) extending out to several hundred eV after the edge. The extent to which the outgoing wave is reflected by a neighbouring atom, and so the intensity of the reflected wave, is partly dependent

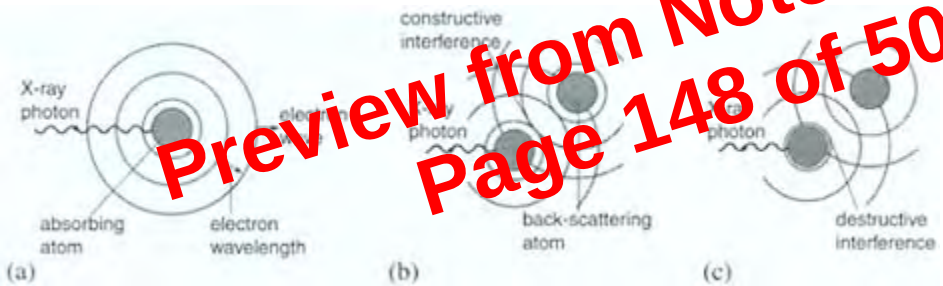

FIGURE 2.23 The EXAFS process: (a) the photoelectron is ejected by X-ray absorption, (b) the outgoing photoelectron wave (solid line) is backscattered constructively by the surrounding atoms (dashed line), and (c) destructive interference between the outgoing and the backscattered wave.

on the scattering factor of that atom. The interference pattern making up the EXAFS thus depends on the *number*, and the *type* of neighbouring atoms, and their *distance* from the absorbing atom.

The EXAFS function is obtained from the X-ray absorption spectrum by subtracting the absorption due to the free atom. A Fourier transform of the EXAFS data gives a **radial distribution function** which shows the distribution of the neighbouring atoms as a function of internuclear distance from the absorbing atom. Shells of neighbours, known as **coordination shells,** surround the absorbing atom. Finally, the radial distribution function is fitted to a series of trial structural models until a structure which best fits the

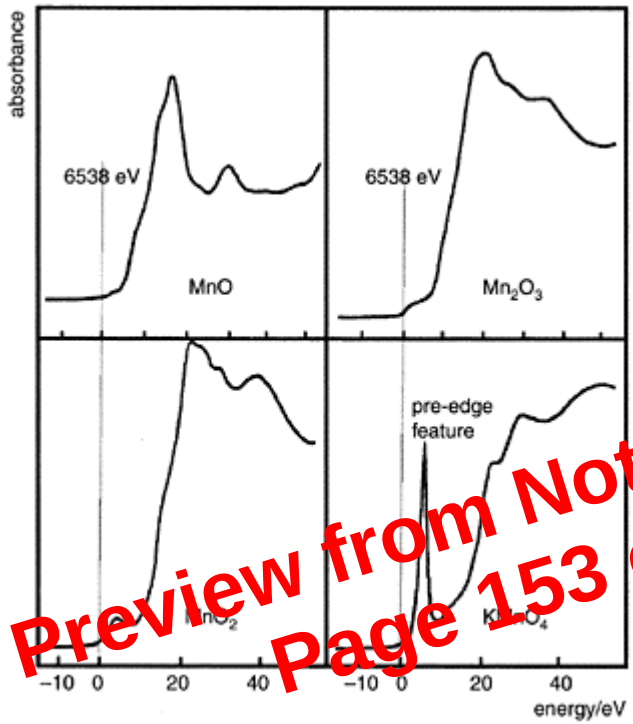

FIGURE 2.26 Mn K-edge XANES data for various manganese oxides. The vertical dashed line is the position of the metal edge. The position of the edge changes, and the pre-edge feature increases, with oxidation state. (Courtesy of Dr. Neville Greaves, University of Aberystwyth.)

The line broadening is due to anisotropic interactions, all of which contain a $(3\cos^2\theta-1)$ term. This term becomes zero when $3\cos^2\theta=1$, or $\cos\theta=(1/3)^{1/2}$, (i.e., $\theta=54°\ 44'$). **Magic angle spinning spectroscopy (MAS NMR)** spins the sample about an axis inclined at this so-called **magic angle** to the direction of the magnetic field and eliminates these sources of broadening, improving the resolution in chemical shift of the spectra. The spinning speed has to be greater than the frequency spread of the signal, if it is less, as may be the case for very broad bands, then a set of so-called "spinning side-bands" are observed, and care is needed in assigning the central resonance.

MAS NMR is often used nowadays as an umbrella term to imply the application of any or all of these techniques in obtaining a solid state NMR spectrum. High resolution

TABLE 2.4 $\sin^2\theta$ values for Cs_2TeBr_6

$\sin^2\theta$
.0149
.0199
.0399
.0547
.0597
.0799
.0947

TABLE 2.5 θ values for NaCl

θ_{hkl}
13°4′
15°51′
23°44′
26°56′
28° 14′
33°7′
36°32′
37°39′
42°0′
45°13′
50°36′
53°54′
55°2′
59°45′

5. X-ray powder data for NaCl is listed in Table 2.5. Determine the Bravais lattice, assuming that it is cubic.

6. Use the data given in Question 5 to calculate a unit-cell length for the NaCl unit cell.

15. Figure 2.34 illustrates the ^{79}Si MAS NMR spectrum of the zeolite faujasite. Use this figure to determine which Si environments are most likely to be present.

16. Figure 2.35 illustrates the ^{29}Si spectrum of the same sample of faujasite as Figure 2.34, but after treatment with $SiCl_4$ and washing with water. What has happened to it?

17. A sample of faujasite was treated with $SiCl_4$ and four ^{27}A1 MAS NMR spectra were taken at various stages afterwards (Figure 2.36). Describe carefully what has happened during the process.

FIGURE 2.34 ^{29}Si MAS NMR spectrum at 79.6 MHz of faujasite of Si/Al=2.61 (zeolite-Y).

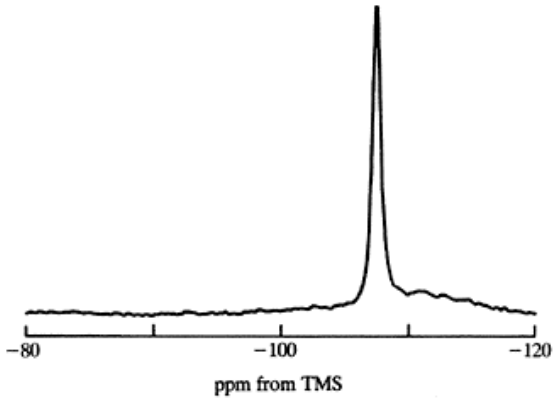

FIGURE 2.35 ^{29}Si MAS NMR spectrum at 79.6 MHz of faujasite of Si/Al=2.61 after successive

3
Preparative Methods

3.1 INTRODUCTION

The interest in the properties of solids and the development of new materials has given rise to the development of a huge variety of methods for preparing them. The method chosen for any solid will depend not only on the composition of the solid but also on the form it is required in for its proposed use. For example, silica glass for fibre optics needs to be much freer of impurities than silica glass used to make laboratory equipment. Some methods may be particularly useful for producing solids in forms that are not the stable form under normal conditions; for example, the synthesis of diamond employs high pressures. Other methods may be chosen because they favour the formation of unusual oxidation states, for example, the preparation of chromium dioxide by the hydrothermal method, or because they promote the production of fine powders or, by contrast, large single crystals. For industrial use, a method that does not employ high temperatures could be favoured because of the ensuing energy savings.

In the preparation of solids, care usually has to be taken to use stoichiometric quantities, pure starting materials, and to ensure that the reaction has gone to completion because it is usually not possible to purify a solid once it has formed.

We do not have space here to discuss all the ingenious syntheses that have been employed over the past few years, so we shall concentrate on those that are commonly used with a few examples of techniques used for solids with particularly interesting properties. The preparation of organic solid state compounds and polymers is not covered because, generally, it involves organic synthesis techniques which is a whole field in itself, and is covered in many organic textbooks.

It is difficult to impose a logical order on such a diverse subject. The chapter begins by considering the most basic, and most commonly used, method of preparing solids, **the ceramic method:** this grand title disguises the fact that it simply means grinding up the reactant solids and heating them hard until they react! We then go on to look at refinements of this method, and ways of improving the uniformity of the reaction and reducing the reaction temperature. The following sections on microwave heating and combustion synthesis discuss alternative methods of inducing solid state reactions. Later sections concentrate on less well-known methods of preparing inorganic solids, such as using high pressures and gas-phase reactions. We also consider some methods used to produce particularly pure solids which are important in the semiconductor industry and the preparation of single crystals.

formation of the gel. Thus the sol-gel method improves the homogeneity of the product but reaction times are still long (note the five day gelling time in the tin dioxide synthesis) and high temperatures (1300 K for silica) are still needed.

Use of microwave ovens instead of conventional heating leads to a speeding-up of reaction in favourable cases.

3.3 MICROWAVE SYNTHESIS

We are all familiar with use of microwave radiation in cooking food where it increases the speed of reaction. Recently this method has been used to synthesize solid state materials such as mixed oxides. The first solid state reaction experiments were performed in modified domestic ovens, and these are still used, but more specialised (and expensive!) ovens have also been developed to give more control over the conditions. We shall briefly consider how microwaves heat solids and liquids because this gives us insight into which reactions will be good candidates for this method.

In a liquid or solid, the molecules or ions are not free to rotate and so the heating is not the result of the absorption of microwaves by molecules undergoing rotational transitions as they would in the gas phase. In a solid or liquid the alternating electric field of the microwave radiation can act in two ways. If charged particles are present that can move freely through the solid or liquid, then these will move under the influence of the field producing an oscillating electric current. Resistance to their movement causes energy to be transferred to the surroundings as heat. This is **conduction heating**. If no particles are present that can move freely, but molecules or units with dipole moments are present, then the electric field acts to align the dipole moments. This effect produces **dielectric heating,** and when it acts on water molecules in food, is generally responsible for the heating/cooking in domestic microwave ovens. The electric field of microwave radiation, like that of all electromagnetic radiation, is oscillating at the frequency of the radiation. The electric dipoles in the solid do not change their alignment instantaneously but with a characteristic time, τ. If the oscillating electric field changes its direction slowly so that the time between changes is much greater than τ then the dipoles can follow the changes. A small amount of energy is transferred to the surroundings as heat each time the dipole realigns but this is only a small heating effect. If the electric field of the radiation oscillates very rapidly, the dipoles cannot respond fast enough and do not realign. The frequency of microwave radiation is such that the electric field changes sign at a speed that is the same order of magnitude as τ. Under these conditions the dipole realignment lags slightly behind the change of electric field and the solid absorbs microwave radiation. This absorbed energy is converted to heat. The quantities governing this process are the dielectric constant (see Chapter 9), which determines the extent of dipole alignment, and the dielectric loss, which governs how efficiently the absorbed radiation is converted to heat.

To use microwave heating in solid state synthesis, at least one component of the reaction mixture must absorb microwave radiation. The speed of the reaction process is then increased by both increasing the rate of the solid state reaction and by increasing the rate of diffusion, which, as we mentioned earlier, is often the rate-limiting step.

hotter region where it can dissolve more silica. In this particular case the autoclave, which is made of steel, can act as the reaction vessel. Because of the corrosive nature of superheated solutions and the possibility of contamination of the product with material from the autoclave walls, it is generally necessary to either line the autoclave with an inert substance, such as teflon, or to perform the reaction in a sealed ampoule in the autoclave.

Chromium Dioxide

Chromium dioxide (CrO_2), which is used on audiotapes because of its magnetic properties (see Chapter 9), contains chromium in the unusual oxidation state of +4. It is prepared by the oxidation of chromium(III) oxide (Cr_2O_3), which is the stable oxide of chromium under normal laboratory conditions. Chromium(III) oxide and chromium trioxide (chromium(VI) oxide CrO_3) are placed in an autoclave with water and heated to 623 K. Oxygen is produced during the reaction, and because the autoclave is sealed, builds up a high partial pressure. (The pressure in the reaction vessel reaches 440 bar.) This high oxygen partial pressure favours the formation of chromium dioxide through the reactions given next:

$$Cr_2O_3+CrO_3=3CrO_2$$

$$CrO_3 = CrO_2 + \frac{1}{2}O_2$$

Zeolites

Zeolites are a class of crystalline **aluminosilicates** (see Chapter 7) based on rigid anionic frameworks with well-defined channels and cavities. These cavities contain exchangeable metal cations, and can hold removable and replaceable guest molecules such as water. The primary building units of zeolites are $[SiO_4]^{4-}$ and $[AlO_4]^{5-}$ tetrahedra linked together by **corner sharing**. Silicon-oxygen tetrahedra are electrically neutral when connected together in a three-dimensional network as in quartz. The substitution of Si(IV) by Al(III) in such a structure, however, creates an electrical imbalance, and to preserve overall electrical neutrality, each $[AlO_4]$ tetrahedron needs a balancing positive charge which is provided by exchangeable cations held electrostatically within the zeolite. It is possible for the tetrahedra to link by sharing two, three, or all four corners, forming a huge variety of different structures.

Naturally occurring zeolite minerals are formed through a hydrothermal process geochemically, and it was demonstrated in the 1940s and 1950s that they could be synthesized in the laboratory by simulating these hydrothermal conditions. A general method of preparing zeolites involves mixing an alkali, aluminium hydroxide and silica sol, or an alkali, a soluble aluminate and silica sol. The silica and aluminate condense to form a gel as in the sol-gel method but the gel is then heated in a closed vessel at temperatures close to 373 K. Under these conditions, zeolites instead of other alumino-silicate phases crystallize out. For example, in the synthesis of a typical zeolite, zeolite A ($Na_{12}[(AlO_2)_{12}(SiO_2)_{12}].27H_2O$) hydrated alumina, $Al_2O_3.3H_2O$, is dissolved in concentrated sodium hydroxide solution. The cooled solution is then mixed with a solution of sodium metasilicate, $Na_2SiO_3.9H_2O$, and a thick white gel forms. The gel is

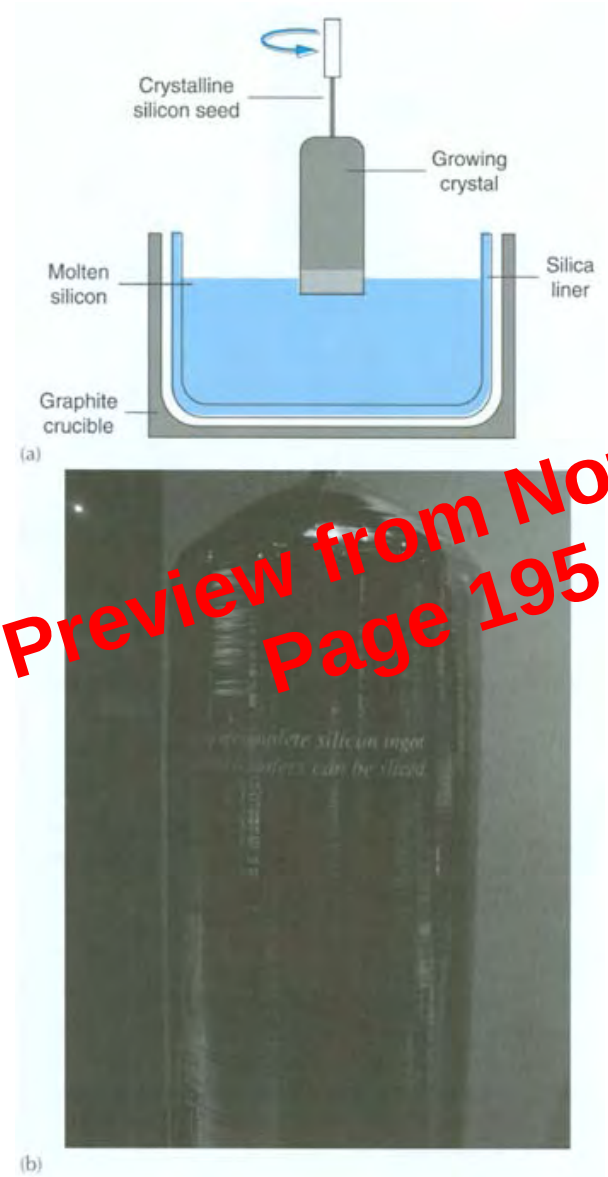

FIGURE 3.14 (a) The Czochralski process for producing a very pure single crystal of silicon; (b) silicon boule. (Photo courtesy of Tonie van Ringelestijn.)

QUESTIONS

1. The Chevrel phase $CuMo_6S_8$ was prepared by a ceramic method. What would be suitable starting materials and what precaution would you have to take?

2. Which synthetic methods would be suitable for producing the following characteristics?
a) A thin film of material.
b) A single crystal.
c) A single crystal containing layers of different material with the same crystal structure.
d) A powder of homogeneous composition.

3. What are the advantages and disadvantages of using the sol-gel method to prepare barium titanate for use in a capacitor?

4. A compound $(NH_4)_2Cr(CrO_4)_2.2NH_3$ is known. How could this be used to prepare $CuCr_2O_4$? What would be the advantages of this method over a ceramic method? Suggest which solvent was used to prepare the ammoniate compound.

5. β-TeI is a metastable phase formed at 465 to 470 K. Suggest an appropriate method of preparation.

6. In hydrothermal processes involving alumina (Al_2O_3), such as the synthesis of zeolites, alkali is added to the reaction mixture. Suggest a reason for this addition.

7. The zeolite ZSM-5 is prepared by heating a mixture of silicic acid, $SiO_2.nH_2O$, NaOH, Al_2SO_4, water, *n*-propylamine, and tetrapropylammonium bromide in an autoclave for several days at 160°C. The product from this reaction is then heated in air. Why is tetrapropylammonium bromide used in the reaction and what is the effect of the subsequent oxidation reaction?

8. Which of the following oxides would be good candidates for microwave synthesis: $CaTiO_3$, $BaPbO_3$, $ZnFe_2O_4$, $Zr_{1-x}Ca_xO_{2-x}$, KVO_3?

9. Crystals of silica can be grown using the chemical vapour transport method with hydrogen fluoride as a carrier gas. The reaction involved is:
$SiO_2(s)+4HF(g)=SiF_4(g)+2H_2O(g)$

10. In the preparation of lithium niobate by CVD, argon-containing oxygen is used as a carrier gas. In the preparation of mercury telluride, the carrier gas was hydrogen. Suggest reasons for these choices of carrier gas.

k+dk is $4/3\pi^2\ V\ ((k+\mathrm{d}k)^3 - k^3)$, which when $(k+\mathrm{d}k)^3$ is expanded, gives a leading term $4/\pi^2\ V\ k^2\mathrm{d}k$. This quantity is the **density of states,** $N(k)\mathrm{d}k$. In terms of the more familiar energy, the density of states $N(E)\mathrm{d}E$ is given by

$$\sqrt{(2m_e)^3 E} \times (V/2\pi^2\hbar^3)\mathrm{d}E$$

A plot of $N(E)\mathrm{d}E$ against E is given in Figure 4.1.

Note that the density of states increases with increasing energy—the higher the energy, the more states there are in the interval dE. In metals, the valence electrons fill up the states from the lowest energy up with paired spins. For sodium, for example, each atom contributes one 3s electron and the electrons from all the atoms in the crystal occupy the levels in Figure 4.1 until all the electrons are used up. The highest occupied level is called the **Fermi level**.

Now let us see how this theoretical density of states compares to reality. Experimentally the density of states can be determined by X-ray emission spectroscopy. A beam of electrons or high energy X-rays hitting a metal can remove core electrons. In sodium, for example, the 2*s* or 2*p* electrons might be removed. The core energy levels are essentially atomic levels and so electrons have been removed from a discrete well-defined energy level. Electrons from the conduction band can now jump down to the energy level emitting X-rays as they do so. The X-ray energy will depend on the level of the conduction band from which the electron has come. A scan across the emitted X-rays will correspond to a scan across the filled levels. The

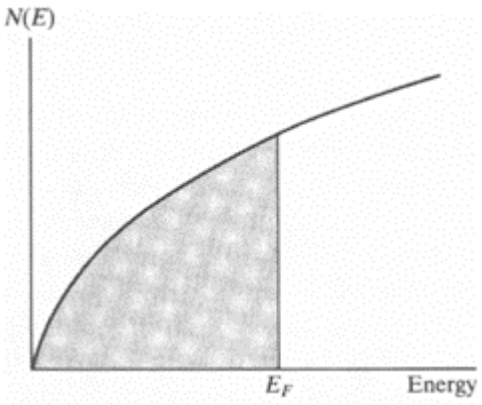

FIGURE 4.1 A density of states curve based on the free electron model. The levels occupied at 0 K are shaded. Note that later in this book, energy is plotted on the vertical axis. In this figure, energy is plotted along the horizontal axis for comparison with experiment.

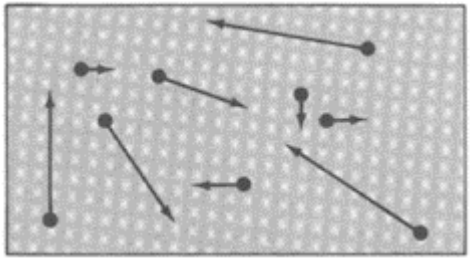

FIGURE 4.4 Electrons in a metal in the absence of an electric field. They move in all directions, but, overall, no net motion occurs in any direction.

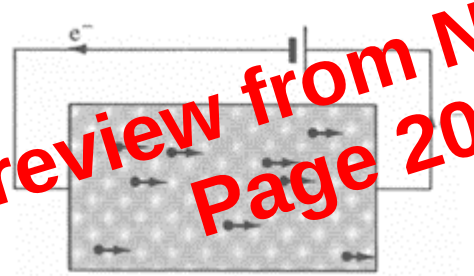

FIGURE 4.5 The sample of Figure 4.4 in a constant electric field, established by placing the rod between the terminals of a battery. The electrons can move in all directions but now their velocities are modified so that each also has a net movement or drift velocity in the left to right direction.

where R is the resistance. It is characteristic of a metal that R increases with increasing temperature (or putting it another way, the conductance, σ, decreases with increasing temperature); that is for a given field, the current decreases as the temperature is raised. There is nothing in our theory yet that will impede the flow of electrons. To account for electrical resistance, it is necessary to introduce the ionic cores. If these were arranged periodically on the lattice sites of a perfect crystal, and they were not able to move, then they would not interrupt the flow of electrons. Most crystals contain some imperfections however and these can scatter the electrons. If the component of the electron's momentum in the field direction is reduced, then the current will drop. In addition, even in perfect crystals the ionic cores will be vibrating. A set of crystal vibrations exists in which the ionic cores vibrate together. These vibrations are called **phonons**. An example

- the structure has an open framework with pathways that the ions can move through;
- the coordination around the ions is also low, so that when they jump from site to site, the coordination changes only changes by a little, affording a route through the lattice with a low activation energy;
- the anions are rather **polarizable;** this means that the electron cloud surrounding an anion is easily distorted, making the passage of a cation past an anion rather easier.

These are properties that are important when looking for other fast-ion conductors.

$RbAg_4I_5$

The special electrical properties of α-AgI inevitably led to a search for other solids exhibiting high ionic conductivity preferably at temperatures lower than 146°C. The partial replacement of Ag by Rb, forms the compound $RbAg_4I_5$. This compound has an ionic conductivity at room temperature of 25 S m^{-1}, with an activation energy of only 0.07 eV. The crystal structure is different from that of α-AgI, but similarly the Rb^+ and I^- ions form a rigid array while the Ag^+ ions are randomly distributed over a network of tetrahedral sites through which they can move.

If a conducting ionic solid is to be useful as a solid electrolyte in a battery, not only must it possess a high conductivity, but also must have *negligible electronic conductivity*. This is to stop the battery short-circuiting: the electrons must only pass through the external circuit, where they can be harnessed to work. $RbAg_4I_5$ has been used as the solid electrolyte in batteries with electrodes made of Ag and RbI_3. Such cells operate over a wide temperature range (−55 to +200°C), have a long shelf life, and can withstand mechanical shock.

A table of ionic conductors that behave in a similar way to α-AgI is given in Table 5.4. Some of these structures are based on a close-packed array of anions and this is noted in the table; the conducting mechanism in these compounds is similar to that in α-AgI. The chalcogenide structures, such as silver sulfide and selenide, tend to demonstrate electronic conductivity as well as ionic, although this can be quite useful in an *electrode material* as opposed to an electrolyte.

5.4.2 FAST-ION CONDUCTORS: OXYGEN ION CONDUCTORS

Stabilized Zirconias

The fluorite structure, as we know from Figure 5.3, has plenty of empty space which can enable an F^- ion to move into an interstitial site. If the activation energy for this process is low enough, we might expect compounds with this structure to show ionic conductivity. Indeed, PbF_2 has a low ionic conductivity at room temperature, but this increases smoothly with temperature to a limiting value of ~500 S m^{-1} at 500°C. Uranium, thorium, and cerium readily form oxides with the fluorite structure, UO_2, ThO_2, and CeO_2, respectively, but zirconium is different. The cubic (fluorite) form of ZrO_2 is only formed at high temperature or when doped with another element.

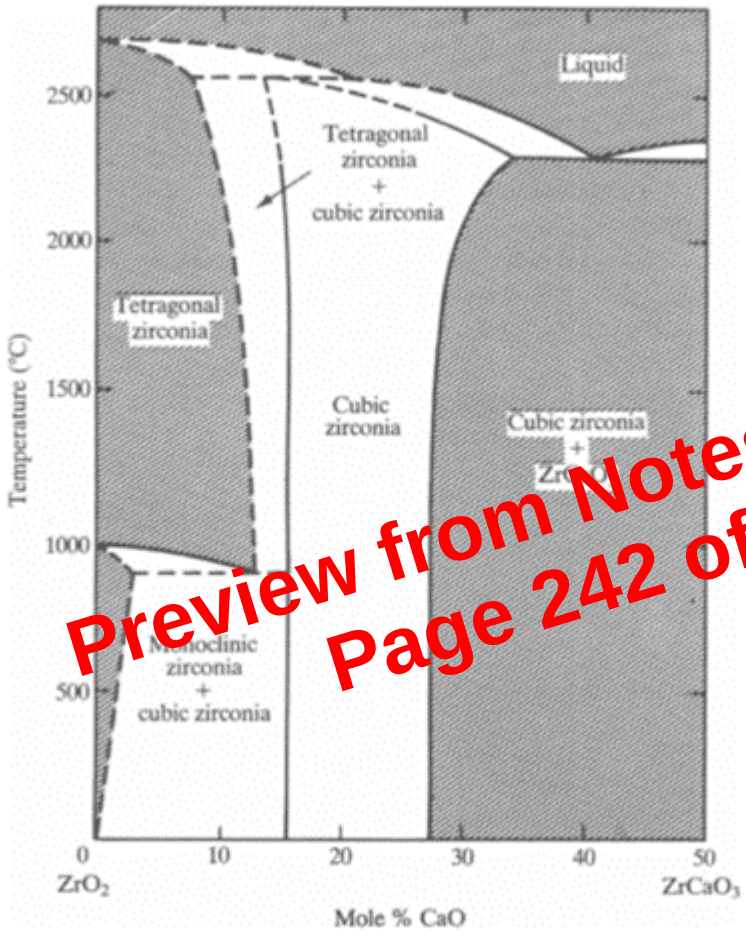

FIGURE 5.11 Phase diagram of the pseudobinary CaO-ZrO_2 system. The cubic calcia-stabilized zirconia phase occupies the central band in the diagram and is stable to about 2400°C.

in the O^{2-} sublattice. Thus, for every Ca^{2+} ion taken into the structure *one* anion vacancy is created. Consequently, these materials are exceptionally good fast-ion conductors of O^{2-} anions (Figure 5.7).

Conductivity maximizes at relatively low concentrations of dopant, but not at the 50% one might expect; this is because there is an elastic interaction between the substituted ion and the vacancy created. The best conductivity seems to be achieved when the crystal lattice is distorted as little as possible (i.e., when the dopant ion is similar in size to the cation it is replacing). Consequently, two of the best oxygen-ion conductors are zirconia

doped with scandia, Sc_2O_3, and ceria doped with gadolinia, Gd_2O_3 (CGO); these are, however, rather expensive. Many other materials are also made with this type of structure, which are based on oxides such as CeO_2, ThO_2, and HfO_2 as well as ZrO_2, and doped with rare earth or alkaline earth oxides: these are collectively known as stabilized zirconias and are widely used in electrochemical systems.

YSZ is the usual material for use in **solid oxide fuel cells**. Another interesting application of stabilized zirconia is in the detection of oxygen, where it is used in both **oxygen meters** and **oxygen sensors,** which are based on a specialized electrochemical cell (Section 5.4.4).

Perovskites

The perovskite structure, ABX_3 (see Chapter 1, Figure 1.44) has two different metal sites which could be substituted with lower valence metal cations leading to oxygen vacancies. Materials based on lanthanum gallate, $LaGaO_3$, have been successfully doped with strontium and magnesium to produce $La_{1-x}Sr_xGa_{1-y}Mg_yO_3$ (LSGM) with similar conductivities to the stabilized zirconias, but at lower temperatures. Using them in oxide ion conducting devices would have the advantage of bringing down the operating temperature.

For some applications, such as the cathode materials in solid oxide fuel cells (see Section 5.4.4), material is needed that can conduct both ions and electrons. The strontium-doped perovskites $LaMnO_3$ (LSM), and $LaCrO_3$ (LSC) have both these properties.

Other Oxygen Ion Conductors

Development of other oxide conductors continues to take place.

- The LAMOX family of oxide conductors, based on $La_2Mo_2O_9$, has high conductivity above 600°C, but tend to be susceptible to reduction by hydrogen.
- The BIMEVOX family of oxide conductors, based on Bi_2O_3, has high conductivity above 600°C.
- The apatite structures, $La_{10-x}M_6O_{26+y}$ (M=Si or Ge), conduct well at very high temperatures.

5.4.3 FAST-ION CONDUCTORS: SODIUM ION CONDUCTORS

β-alumina

β-alumina is the name given to a series of compounds that demonstrate fast-ion conducting properties. The parent compound is sodium β-alumina, $Na_2O.11Al_2O_3$ ($NaAl_{11}O_{17}$), and is found as a by-product from the glass industry. (The compound was originally thought to be a polymorph of Al_2O_3, and was named as such—it was only later found to contain sodium ions! However, the original name has stuck.) The general formula for the series is $M_2O.nX_2O_3$, where *n* can range from 5 to 11: M is a monovalent cation such as $(\text{alkali metal})^+$, Cu^+, Ag^+, or NH_4^+, and X is a trivalent cation Al^{3+}, Ga^{3+}, or

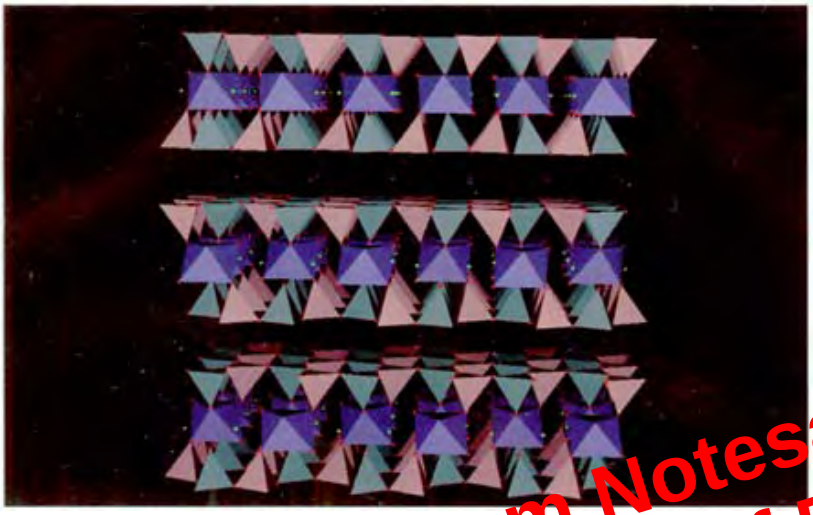

FIGURE 1.35 The structure of biotite. Key: Mg, green; Si, grey; O, red; Na, purple; Al, pink; F, blue.

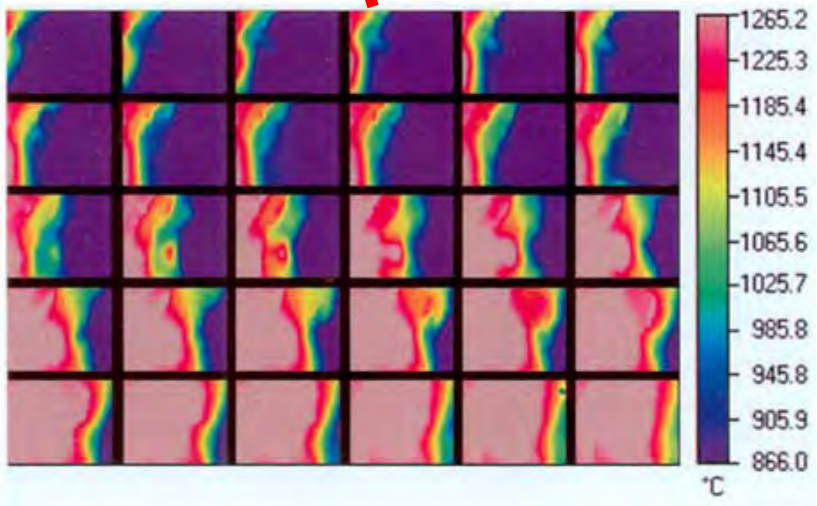

FIGURE 3.4 Thermal images of the synthesis wave moving through a pellet of MgO, Fe, Fe_2O_3, and $NaClO_4$. Each image is of dimension 3×2 mm. Images were captured at 0.06 s

To increase the rate of reaction, an expensive Pt catalyst is incorporated into the carbon electrodes. If the electrolyte allows the passage of H^+ ions, the cell reaction can be written:

A	**B**	**C**
$H_2(g)$//Pt/C electrode//	hydrogen electrolyte	//Pt/C electrode//$O_2(g)$

Anode A: $H_2=2H^++2e^-$
Cathode C: $½O_2+2H^++2e^-=H_2O$

The theoretical emf for this cell, calculated from the Gibbs function for the decomposition of water, is $E^\circ = 1.229$ V at 298 K, but this decreases with temperature to about 1 V at 500 K. A compromise in cell design is therefore always needed between the voltage generated and an operating temperature high enough to maintain a fast reaction.

The oxygen supply comes simply from the air, but a major drawback is the supply, transportation and storage of the hydrogen. The current infrastructure of fuel stations is for the supply of liquid fuel: petrol (gasoline) and diesel. Hydrogen, a gas at room temperature, is the least dense of all the elements so has to be compressed or liquefied in order to store it in a manageable volume. Compressed hydrogen needs a strong tank that can withstand the high pressures involved; these cylinders are very heavy. Liquefied hydrogen requires cooling and must be kept very cold (boiling point is −253°C), so the tanks must be extremely well insulated. Research is under way to develop materials, such as carbon nanotubes, which will store large amounts of hydrogen and release it when needed. Although hydrogen is probably less dangerous than a liquid hydrocarbon fuel, public perception about its safety needs to be overcome: many people have seen old footage of the hydrogen-filled Hindenberg airship exploding on landing.

Hydrogen also has to be generated; very pure hydrogen, required by some fuel cells, is produced electrolytically, which is an expensive process unless cheap sources of electricity can be found, such as solar energy or hydroelectric power. The alternative is to use a **reforming reaction,** where hydrogen-rich sources, such as methane or methanol, are reacted with steam to produce hydrogen and carbon dioxide. To avoid the transport and storage problems, hydrogen can also be produced *in situ* using a reformer and fed directly into the fuel cell. The reforming reaction has its own problems, in that the catalyst is poisoned by sulfur in the fuel. In addition, small quantities of carbon monoxide are produced along with the hydrogen in the reforming reaction, and this also poisons the Pt catalyst in the fuel cell thereby reducing its efficiency.

Fuel cells have been around for quite a long time; it was in 1839 that William Grove, a Welsh physicist, made the first working fuel cell, but not until 1959 that Tom Bacon at Cambridge University produced a stack of 40 alkaline fuel cells that produced 5 kW of power. Around the same time, Willard Grubb and Leonard Niedrach at General Electric developed a conducting membrane fuel cell with a Pt catalyst on a Ti gauze which was used in the Gemini earth-orbit space programme. By 1965, Pratt & Whitney had improved (longer life) the alkaline fuel cells (AFC) for use in the Apollo missions where they provided both power and drinking water for the astronauts. In 1983, Ballard Power (Canada) was established, and in 1993, unveiled the first fuel cell buses which went into

It is vital that the solid oxide electrolyte can withstand the extreme conditions of hydrogen at the anode at 800°C or above. Under these conditions, many oxides would be reduced, liberating electrons and thus leading to unwanted electronic conductivity.

The cathode materials used have to conduct both oxide ions and electrons satisfactorily, but, in addition, for compatibility, they must have similar thermal expansion coefficients as the electrolyte. The strontium-doped perovskite, LSM (see Section 5.4.2), is one of the materials of choice.

FIGURE 5.20 Industrial-sized 220 kW solid oxide fuel cell made by Siemens. (Courtesy of Siemens PG CTET: Stationary Fuel Cells, Europe.)

Proton Exchange Membrane Fuel Cells (PEM)

There is currently great interest in the PEM cells which operate at much lower temperatures (80°C). Here the electrolyte is a conducting polymer membrane (see Chapter 6), usually Nafion, which is a sulfonated fluoropolymer made by Dupont, strengthened by Gore-Tex™. The strongly acidic $-SO_2OH$ group allows the passage of H^+ ions, but not of atoms or electrons. Output is typically 1 V at 80°C; with a current flow of 0.5 A cm^{-2}, this drops to 0.5 V because of ohmic losses. A membrane of 1 m^2 provides about 1 kW. To produce the correct power output, a number of cells are placed together to form a **stack**. Most car manufacturers now have prototype zero emission vehicles (Figure 5.21), and the first hydrogen fuel-cell consumer vehicle—a Nissan 4×4 pick-up truck—went on sale in the USA in 2005.

250 kilowatt fuel cells are made which provides enough heat and electricity to power industry, and indeed for establishments needing high reliability and backup power supplies, such as banks and hospitals (Figure 5.20). Smaller systems (7 kW), about the size of a refrigerator, are produced that can provide all the power necessary for a house and the heat produced can also be harnessed to provide hot water. Fuel cells are still used to power the space shuttle. Because of a European Union initiative, DaimlerChrysler built between 20 and 30 fuel cell buses for use in eight European cities, three of which were destined for London (2004). The buses run on compressed hydrogen stored in tanks in the

light are unaffected by the developer (unless the film is developed for a very long time, when eventually they will be reduced and a fogged picture results). The final stage in producing a negative is to dissolve out the remaining light-sensitive AgBr. This is done using 'hypo'—sodium thiosulfate ($Na_2S_2O_3$), which forms a water soluble complex with Ag^+ ions.

5.6 COLOUR CENTRES

During early research in Germany, it was noticed that if crystals of the alkali halides were exposed to X-rays, they became brightly coloured. It was thought that the colour was associated with a defect known then as a **Farbenzentre (colour centre),** now abbreviated as **F-centre**. Since then, it has been found that many forms of high energy radiation (UV, X-rays, neutrons) will cause F-centres to form. The colour produced by the F-centres is always characteristic of the host crystal, so, for instance, NaCl becomes deep yellowy-orange, KCl becomes violet, and KBr becomes blue-green.

Subsequently, it was found that F-centres can also be produced by heating a crystal in the vapour of an alkali metal: this gives a clue to the nature of these defects. The excess alkali metal atoms diffuse into the crystal and settle on cation sites. At the same time, an equivalent number of anion site vacancies are created and ionisation gives an alkali metal cation with an electron trapped at the anion vacancy (Figure 5.24). In fact, it does not even matter which alkali-metal is used, if NaCl is heated with potassium, the colour of the F-centre does not change because

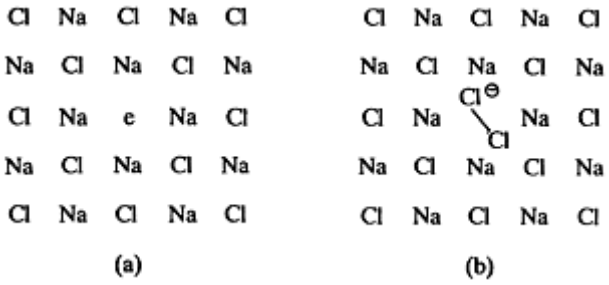

FIGURE 5.24 (a) The F-centre, an electron trapped on an anion vacancy; (b) H-centre.

it is characteristic of the electron trapped at the anion vacancy in the host halide. Work with Electron Spin Resonance spectroscopy, ESR, has confirmed that F-centres are indeed unpaired electrons trapped at vacant lattice (anion) sites.

The trapped electron provides a classic example of an 'electron in a box'. A series of energy levels are available for the electron, and the energy required to transfer from one level to another falls in the visible part of the electromagnetic spectrum, hence the colour of the F-centre. There is an interesting natural example of this phenomenon: The mineral

fluorite (CaF_2) is found in Derbyshire, United Kingdom where it is known as ‘Blue John’, and its beautiful blue-purple colouration is due to the presence of F-centres.

Many other colour centres have now been characterized in alkali halide crystals. The **H-centre** is formed by heating, for instance, NaCl in Cl_2 gas. In this case, a $[Cl_2]^-$ ion is formed and occupies a single anion site (Figure 5.24(b)). F-centres and H-centres are perfectly complementary—if they meet, they cancel one another out!

Another interesting natural example of colour centres lies in the colour of smoky quartz and amethyst. These semi-precious stones are basically crystals of silica, SiO_2, with some impurities present. In the case of smoky quartz, the silica contains a little aluminium impurity. The Al^{3+} substitutes for the Si^{4+} in the lattice, and the electrical neutrality is maintained by H^+ present in the same amount as Al^{3+}. The colour centre arises when ionising radiation interacts with an $[AlO_4]^{5-}$ group, liberating an electron which is then trapped by H^+:

$$[AlO_4]^{5-}+H^+=[AlO_4]^{4-}+H$$

The $[AlO_4]^{4-}$ group is now electron-deficient and can be considered as having a ‘hole’ trapped at its centre. This group is the colour centre, absorbing light and producing the smoky colour. In crystals of amethyst, the impurity present is Fe^{3+}. On irradiation, $[FeO_4]^{4-}$ colour centres are produced which absorb light to give the characteristic purple coloration.

5.7 NON-STOICHIOMETRIC COMPOUNDS

5.7.1 INTRODUCTION

Previous sections of this chapter have shown that it is possible to *introduce* defects into a perfect crystal by adding an impurity. Such an addition causes point defects of one sort or another to form, but they no longer occur in complementary pairs. Impurity-induced defects are said to be **extrinsic**. We have also noted that when assessing what defects have been created in a crystal, it is important to remember that the overall charge on the crystal must always be zero.

Colour centres are formed if a crystal of NaCl is heated in sodium vapour; sodium is taken into the crystal, and the formula becomes $Na_{1+x}Cl$. The sodium atoms occupy cation sites, creating an equivalent number of anion vacancies; they subsequently ionize to form a sodium cation with an electron trapped at the anion vacancy. The solid so formed is a **non-stoichiometric compound** because the ratio of the atomic components is no longer the simple integer that we have come to expect for well-characterized compounds. A careful analysis of many substances, particularly inorganic solids, demonstrates that it is common for the atomic ratios to be non-integral. Uranium dioxide, for instance, can range in composition from $UO_{1.65}$ to $UO_{2.25}$, certainly not the perfect UO_2 that we might expect! Many other examples exist, some of which we discuss in some detail.

What kind of compounds are likely to be non-stoichiometric? ‘Normal’ covalent compounds are assumed to have a fixed composition where the atoms are usually held together by strong covalent bonds formed by the pairing of two electrons. Breaking these bonds usually takes quite a lot of energy, and so under normal circumstances, a particular

compound does not show a wide range of composition; this is true for most molecular organic compounds, for instance. Ionic compounds also are usually stoichiometric because to remove or add ions requires a considerable amount of energy. We have seen, however, that it is possible to make ionic crystals non-stoichiometric by doping them with an impurity, as with the example of Na added to NaCl. Another mechanism also exists, whereby ionic crystals can become non-stoichiometric: if the crystal contains an element with a variable valency, then a change in the number of ions of that element can be compensated by changes in ion charge; this maintains the charge balance but alters the stoichiometry. Elements with a variable valency mostly occur in the transition elements, the lanthanides and the actinides.

In summary, non-stoichiometric compounds can have formulae that do not have simple integer ratios of atoms; they also usually exhibit a range of composition. They can be made by introducing impurities into a system, but are frequently a consequence of the ability of the metal to exhibit variable valency. Table 5.5 lists a few non-stoichiometric compounds together with their composition ranges.

TABLE 5.5 Approximate composition ranges for some non-stoichiometric compounds

Compound		Composition range[a]
TiO_x	[≈TiO]	$0.65<x<1.25$
	[≈TiO_2]	$1.998<x<2.000$
VO_x	[≈VO]	$0.79<x<1.29$
Mn_xO	[≈MnO]	$0.848<x<1.000$
Fe_xO	[FeO]	$0.833<x<0.957$
Co_xO	[≈CoO]	$0.988<x<1.000$
Ni_xO	[≈NiO]	$0.999<x<1.000$
CeO_x	[≈Ce_2O_3]	$1.50<x<1.52$
ZrO_x	[≈ZrO_2]	$1.700<x<2.004$
UO_x	[≈UO_2]	$1.65<x<2.25$
$Li_xV_2O_5$		$0.2<x<0.33$
Li_xWO_3		$0<x<0.50$
TiS_x	[≈TiS]	$0.971<x<1.064$
Nb_xS	[≈NbS]	$0.92<x<1.00$
Y_xSe	[≈YSe]	$1.00<x<1.33$
V_xTe2	[≈VTe_2]	$1.03<x<1.14$

[a]Note that all composition ranges are temperature dependent and the figures here are intended only as a guide.

and O, 16.00. One mole of FeO weighs (55.85+16.00) g= 0.07185 kg; four moles weigh (4×0.07185) kg; and four formula units weigh (4× 0.07185)/N_A kg=4.773×10^{-25} kg, where **Avogadro's number,** N_A=6.022×10^{23} mol^{-1}.

The sample under consideration has an Fe:O ratio of 0.945. Assume, in the first instance, that it has *iron vacancies:* The unit cell contents in this case will be (4×0.945)=3.78Fe and 4O. The mass of the contents will be [(3.78×55.85)+(4×16.00)]/(N_A×10^3) kg. Dividing by the volume of the unit cell, we obtain a value of 5.742×10^3 kg m^{-3} for the density. If instead the sample possesses *interstitial oxygens*, the ratio of oxygens to iron in the unit cell will be given by 1/0.945=1.058. The unit cell in this case will contain 4Fe and (4×1.058)= 4.232 O. The mass of this unit cell is given by: [(4×55.85)+(4.232×16.00)]/(N_A ×10^3) kg, giving a density of 6.076×10^3 kg m^{-3}. Comparing the two sets of calculations with the experimentally measured density of 5.728×10^3 kg m^{-3}, it is clear that this sample contains *iron vacancies* and that the formula should be written as $Fe_{0.945}O$. A table of densities is drawn up for FeO in Table 5.6.

It is found to be characteristic of most non-stoichiometric compounds that *the unit cell size varies smoothly with composition but the symmetry is unchanged*. This is known as **Vegard's Law**.

In summary, non-stoichiometric compounds are found to exist over a range of composition, and throughout that range the unit cell length varies smoothly with no change of symmetry. It is possible to determine whether the non-stoichiometry is accommodated by vacancy or interstitial defects using density measurements.

Electronic Defects in FeO

The discussion of the defects in FeO has so far been only structural. Now we turn our attention to the balancing of the charges within the crystal. In principle the compensation for the iron deficiency can be made either by oxidation of some Fe(II) ions *or* by reduction of some oxide anions. It is energetically more favourable to oxidise Fe(II). For each Fe^{2+} vacancy, *two* Fe^{2+} cations must be oxidised to Fe^{3+}. In the overwhelming majority of cases, defect creation involves changes in the cation oxidation state. In the case of metal excess in simple compounds, we would usually expect to find that neighbouring cation(s) would be reduced.

In a later section we will look at some general cases of non-stoichiometry in simple oxides, but before we do that we will complete the FeO story with a look at its detailed structure.

parallel to it will be the central horizontal plane of the unit cell at b=½. This is drawn in Figure 5.28(c), and again we notice that every other atom along every third diagonal plane is missing. This is true throughout the structure. In the figure, the unit cell of a perfect NaCl type structure is marked on (a), whereas the boundaries of the new unit cell, taking the ordered defects into account, are marked on (b) and (c). The new unit cell of the superlattice is **monoclinic** (see Chapter 1) because the angle in the *xz* plane (β) is not equal to 90°. This structure is unusual in that it appears to be stoichiometric, but, in fact, contains defect vacancies on both the anion and cation sublattices.

As discussed in Chapter 4, unusually for a transition metal monoxide, $TiC_{1.00}$ demonstrates metallic conductivity. The existence of the vacant sites within the TiO structure is thought to permit sufficient contraction of the lattice that the 3*d* orbitals on titanium overlap, thus broadening the conduction band and allowing electronic conduction.

When titanium monoxide has the limiting formula $TiC_{1.25}$, it has a different defect structure, still based on the NaCl structure, but with *all* the oxygens present and one in every five titaniums missing (Figure 5.29). The pattern of the titanium vacancies is shown in Figure 5.30, which is a layer of the type in Figure 5.28 but

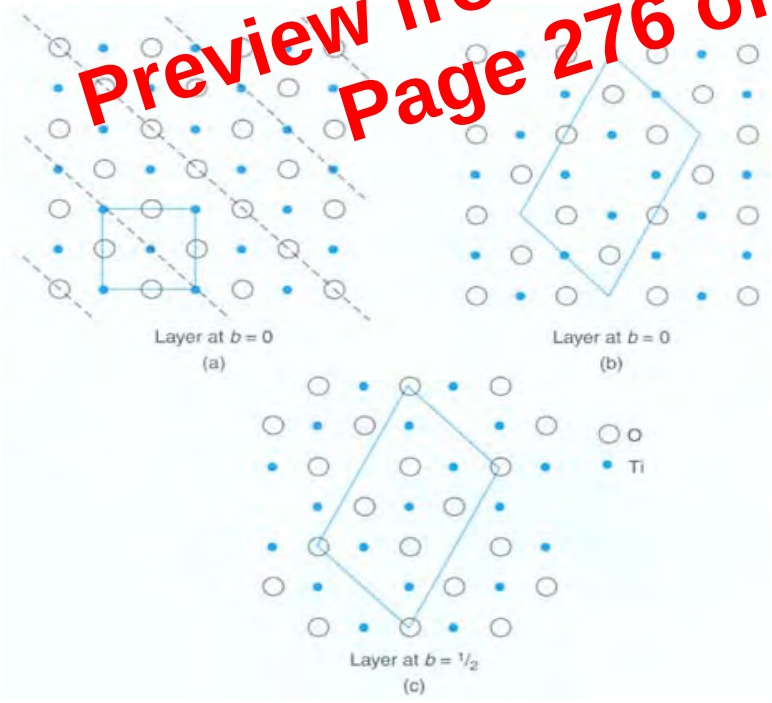

FIGURE 5.28 Layers parallel to the horizontal planes of Figure 1.31. (a) The hypothetical TiO structure of the NaCl type shown in Figure 1.31; the

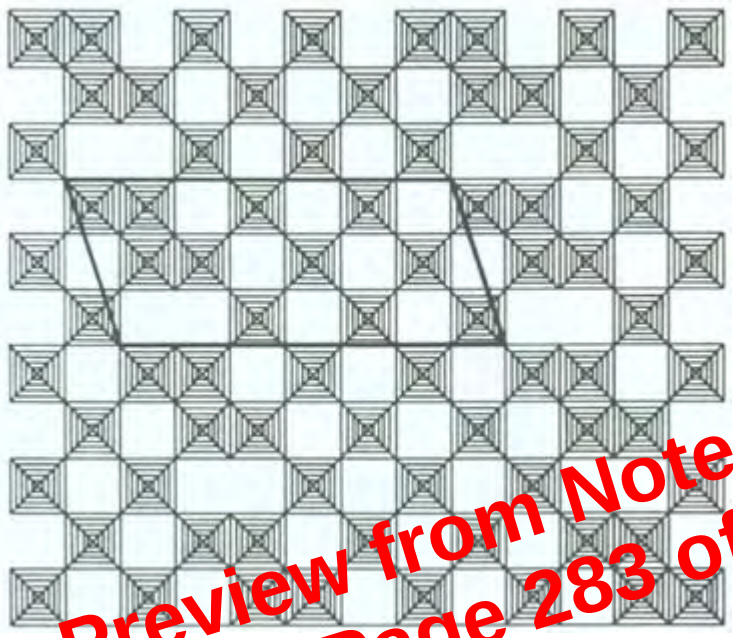

FIGURE 5.34 A member of the W_nO_{3n-1} homologous series with the projection of a unit cell marked.

If the structures shear in such a way that groups of six octahedra share edges regularly throughout the structure, then homologous series with the general formula M_nO_{3n-2} are formed.

The homologous series for oxygen deficient TiO_2 is given by the formula Ti_nO_{2n-1}. In this case, the octahedra along the CS planes are joined to each other by sharing *faces*, whereas in the unreduced parts of the TiO_2 structure the octahedra share edges as in rutile.

5.8.2 PLANAR INTERGROWTHS

Many systems show examples of intergrowth where a solid contains regions of more than one structure with clear solid-solid interfaces between the regions. Epitaxy (see Chapter 3) is an example of such a phenomenon with great technological interest for the production of circuits and ‘smart’ devices. The zeolites ZSM-5 and ZSM-11 can form intergrowths (see Chapter 7), as can the barium ferrites (see Chapter 9). We will only look at one example here that of intergrowths in the **tungsten bronzes**. The term *bronze* is applied to metallic oxides that have a deep colour, metallic lustre and are either metallic conductors or semiconductors. The sodium-tungsten bronzes, Na_xWO_3, have colours that range from yellow to red and deep purple depending on the value of x.

Going back now to the non-stoichiometric oxides, in the excess metal monoxides of type A and type B, we saw that extra electrons have to compensate for the excess metal in the structure. Figure 5.41 illustrates that these could be associated either with an anion vacancy or alternatively they could be associated with metal cations within the structure. Although we have described this association as reducing neighbouring cations, this association can be quite weak, and these electrons can be free

TABLE 5.8 Properties of the first-row transition element monoxides

Element	Ca	Sc	Ti	V	Cr	Mn	Fe	Co	Ni	Cu	Zn
Structure of stoichiometric oxide MO	NaCl structure	Does not exist	Defect NaCl 1/6 vacancies	Defect NaCl	Does not exist	NaCl structure	NaCl structure[a]	NaCl structure	NaCl structure	PtS structure	Wurtzite structure (NaCl at high pressure)
Defect structure			$Ti_{1-\delta}O$	$V_{1-\delta}O$		$Mn_{1-\delta}O$	$Fe_{1-\delta}O$	$Co_{1-\delta}O$	$Ni_{1-\delta}O$		$Zn_{1+\delta}O$
			Ti vacancies (inter growths of $TiO_{1.00}$ and $TiO_{1.25}$ structures)	V vacancies and tetra hedral V inters titials in defect clusters		Mn vacancies	Fe vacancies and tetrahedral Fe interstitials in defect clusters	Co vacancies	Ni vacancies		Interstitial Zn
Conductivity of stoichiometric compound			Metallic	Metallic <120 K		Insulator	Insulator	Insulator	Insulator		Insulator
Conductivity of non-stoichiometric compound			Metallic	Metallic		*p*-type hopping semiconductor	*p*-type	*p*-type	*p*-type		*n*-type
Magnetism (see Chapter 9)			Diamagnetic	Diamagnetic		Paramagnetic μ=5.5 μ_B (antiferromagnetic when cooled, T_N= 122 K)	Paramagnetic (antiferromagnetic when cooled, T_N=198 K)	Antiferromagnetic (T_N= 292 K)	Antiferromagnetic T_N= 530 K)		

[a]Exactly stoichiometric FeO is never found.

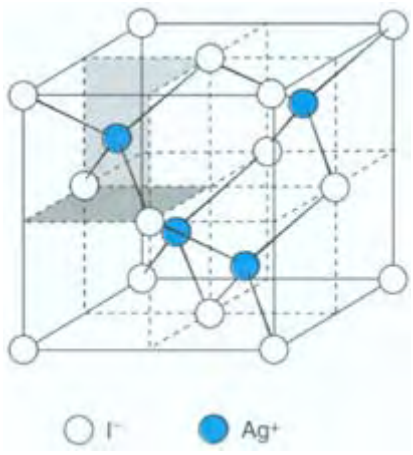

FIGURE 5.43 The zinc blende structure of γ-AgI.

9. The compounds in Table 5.4 mostly contain either I^- ions or ions from the heavier end of Group 16. Explain.

10. Undoped β-alumina demonstrates a maximum conductivity and minimum activation energy when the sodium excess is around 20 to 30 mole%. Thereafter, further increase in the sodium content causes the conductivity to decrease. By contrast, β-alumina crystals doped with Mg^{2+} have a much higher conductivity than do undoped crystals. Explain these observations.

11 Confirm the presence of iron vacancies for a sample of wustite which has a unit cell dimension of 428.2 pm, an Fe:O ratio of 0.910 and an experimental density of 5.613×10^3 kg m^{-3}.

12. How does the change in lattice parameter of 'FeO' with iron content corroborate the iron vacancy model and refute an oxide interstitial model?

13. How would you expect the formation of colour centres to affect the density of the crystal?

14. Figure 5.44 depicts the central section of a possible defect cluster for FeO. (a) Determine the vacancy:interstitial ratio for this cluster, (b) Assuming that this section is surrounded by Fe ions and oxide ions in octahedral sites as in the Koch-Cohen cluster, determine the formula of a sample made totally of such clusters, (c) Determine the numbers of Fe^{2+} and Fe^{3+} ions in octahedral sites.

15. Use Figure 5.28 to confirm that TiO is a one-sixth defective NaCl structure, by counting up the atoms in the monoclinic cell.

17. How would you expect charge neutrality to be maintained in $TiO_{1.25}$?

18. Take a simple case where *two* metal oxide octahedra wish to eliminate oxygen by sharing. How does the formula change as they (i) share a corner, (ii) share an edge, (iii) share a face?

19. Figure 5.45 shows a member of the homologous series, W_nO_{3n-1}. To what formula does it correspond?

20. ZnO is a type B (excess metal) material. What do you expect to happen to its electronic properties if it is doped with Ga_2O_3 under reducing conditions?

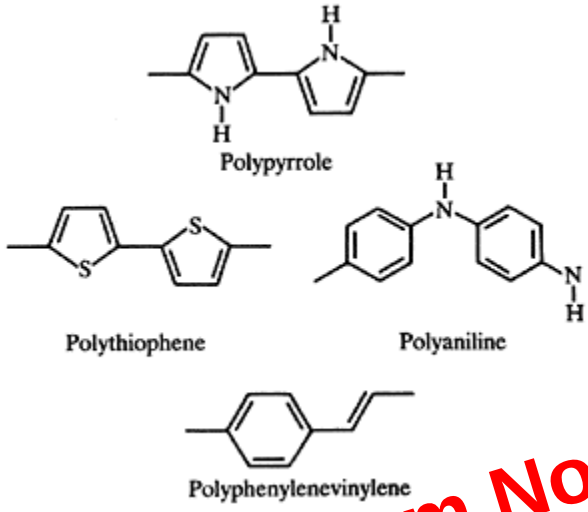

FIGURE 6.4 Repeating units of some conducting polymers.

ductivity are similar to those of polyacetylene. These polymers are, however, less sensitive to oxygen and by attaching suitable side chains can be made soluble in nonpolar organic solvents and thereby easier to process. As for polyacetylene, the conductivity of these polymers is sensitive to doping. This is exploited in polypyrrole gas sensors, which are based on the variation of conductivity of a thin polymer film when exposed to gases such as NH_3 and H_2S. Doped conducting polymers can also be used as a metallic contact in organic electronic devices. The most promising commercial applications of conjugated polymers such as the LED described in Section 6.2.3, however, use undoped polymer.

6.2.2 BONDING IN POLYACETYLENE AND RELATED POLYMERS

In small conjugated alkenes such as butadiene with alternate double and single bonds, the π electrons are delocalised over the molecule. If we take a very long conjugated olefin, we might expect to obtain a band of π levels, and if this band were partly occupied, we would expect to have a one-dimensional conductor. Polyacetylene is just such a conjugated long chain polymer. Now if polyacetylene consisted of a regular evenly spaced chain of carbon atoms, the highest occupied energy band, the π band, would be half full and polyacetylene would be an electrical conductor. In practice, polyacetylene demonstrates only modest electrical conductivity, comparable with semiconductors such as silicon: the *cis* form has a conductivity of the order 10^{-7} S m^{-1} and the *trans* form, 10^{-3} S m^{-1}. The crystal structure is difficult to determine accurately, but diffraction measurements indicate that an alternation in bond lengths of about 6 pm occurs. This is much less than would be expected for truly alternating single and double bonds (C—C, 154 pm in ethane; C=C, 134 pm in ethene). Nonetheless, this does indicate that the

occurs. With very good electron donors such as alkali metals, one electron per TCNQ is transferred and the acceptor band is full. Thus, $K^+(TCNQ)^-$ is an insulator.

At low temperatures, TTF-TCNQ suffers a periodic distortion and so its conductivity drops.

6.3.2 TWO-DIMENSIONAL MOLECULAR METALS

Polyacetylene and TTF-TCNQ are all pretty well described as one-dimensional electronic conductors, because little interaction occurs between chains in the crystal. Another class of molecular metals exists, however, which, while appearing to resemble these solids, are less unambiguously defined as one-dimensional.

For example, tetramethyl-tetraselenofulvalene (TMTSF), Figure 6.8, forms a series of salts with inorganic anions. The crystals of these salts contain stacks of TMTSF molecules and the TMTSF molecules carry a fractional charge (0.5+). As expected, these salts have high electronic conductivities at room temperatures. Unlike TTF-TCNQ, however, $(TMTSF)_2^+(ClO_4)^-$ and other similar salts remain highly conducting at low temperatures and indeed at very low temperatures become superconducting. The reason for this appears to be that significant overlap occurs between stacks. As a result, the one-dimensional model is not as valid as for TTF-TCNQ, and in particular, Peierls' theorem no longer holds.

Other materials of this type with significant interaction between chains include $(SN)_x$ and $Hg_{3-x}AsF_6$, both of which become superconducting at low temperatures.

Other similar compounds, instead of containing chain-like stacks of organic molecules, contain flat organic ring compounds stacked so that molecular orbitals on different molecules overlap to form bands. The organic molecules form planes

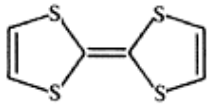

TTF

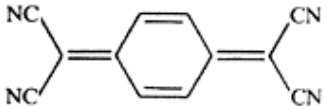

TCNQ

(a)

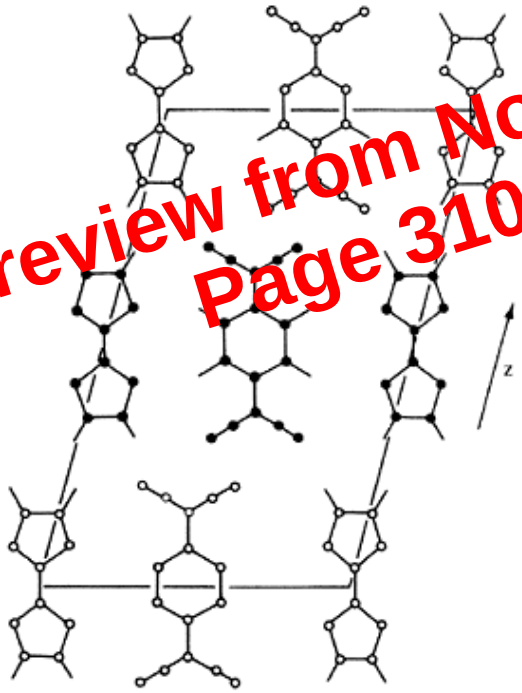

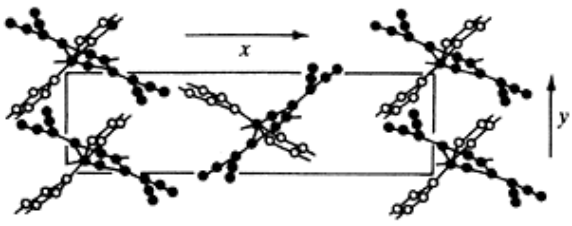

(b)

FIGURE 6.7 Structures of (a) TTF and TCNQ and (b) solid TTF-TCNQ, showing alternate stacks of TTF and TCNQ molecules.

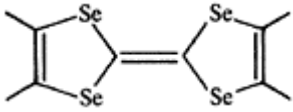

FIGURE 6.8 Structure of tetramethyl-tetraselenofulvalene (TMTSF).

separated by layers of anions. Electrons are delocalised over the planes of organic molecules. A typical example is bis(ethylenedithio)tetrathiofulvalene (BEDT-TTF).

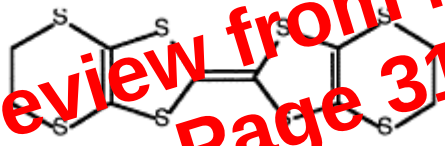

This forms molecular metals $(BEDT\text{-}TTF)_2X$ with a variety of anions including $[Cu(NCS)_2]-$, I_3^-, AuI_2^-, IBr_2^-, $[Cu(N(CN)_2)X]^-$(X=Cl or Br), $[Cu(CN)_3]^-$, $GaCl_4^-$, $SF_5CH_2CF_2SO_3^-$. The packing arrangement varies with the anion. Figure 6.9 depicts the arrangement for β-$(BEDT\text{-}TTF)_2I_3$, which contains layers of I_3^- ions.

solvent is a mixture of dimethoxyethane (DME) and tetrahydrofuran (THF). The setup is illustrated in Figure 6.10.

When the circuit is complete, lithium metal from the lithium electrode dissolves giving solvated ions, and solvated ions in the solution are deposited in the titanium disulfide. These ions intercalate into the disulfide, and electrons from the external circuit balance the charge. Thus, the two electrode reactions are:

$$Li(s)=Li^{+}(solv)+e^{-} \quad (6.1)$$

and

$$xLi^{+}(solv)+TiS_2(s)+xe^{-}=Li_xTiS_2(s) \quad (6.2)$$

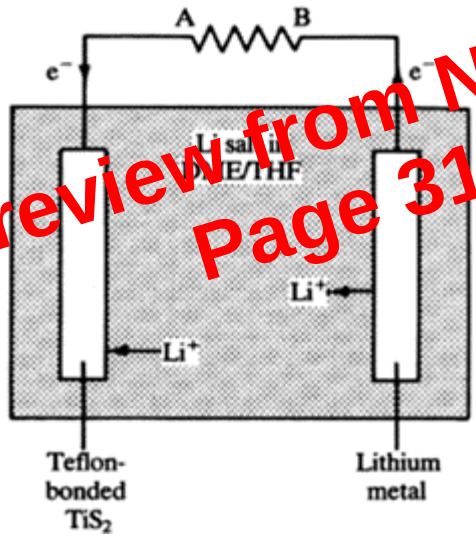

FIGURE 6.10 The Li-TiS_2 battery during a discharge phase.

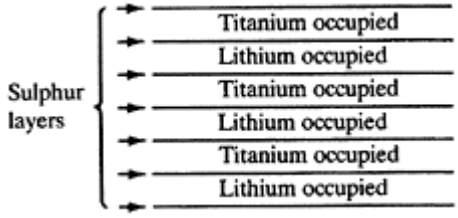

FIGURE 6.11 Occupation pattern of octahedral holes between close-packed layers of sulfur atoms in $LiTiS_2$.

zero, and electrons are thus readily promoted to the upper band. The band structure for graphite is illustrated in Figure 6.13.

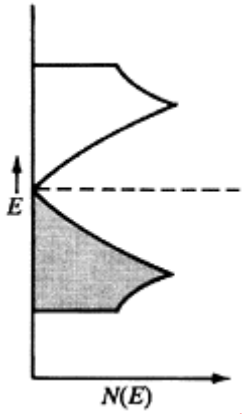

FIGURE 6.13 Band structure of graphite.

Because the density of states is low at the Fermi level, the conductivity is not as high as that for a typical metal. It can, however, be increased as you will now see.

6.5.2 INTERCALATION COMPOUNDS OF GRAPHITE

Because the bonding between layers in graphite is weak, it is easy to insert molecules or ions into the spaces between layers. The solids produced by reversible insertion of such guest molecules into lattices are known as intercalation compounds, and although originally applied to layered solids the term is now taken to include other solids with similar host-guest interactions. Since the 1960s, attention has been paid to intercalation compounds as of possible importance as catalysts and as electrodes for high energy-density batteries (see previous section).

Many layered solids form intercalation compounds, but graphite is particularly interesting because it forms compounds with both electron donors and electron acceptors. Amongst electron donors, the most extensively studied are the alkali metals. The alkali metals enter graphite between the layers and produce strongly coloured solids in which the layers of carbon atoms have moved farther apart. For example, potassium forms a golden compound KC_8 in which the interlayer spacing is increased by 200 pm. The potassium donates an electron to the graphite (forming K^+) and the conductivity of the graphite now increases because it has a partially full anti-bonding band.

The first intercalation compound was made in 1841. This contained sulfate, an electron acceptor. Since then, many other electron acceptor intercalation compounds have been made with, for example, NO_3^-, CrO_3, Br_2, $FeCl_3$, and AsF_5. In these compounds, the graphite layers donate electrons to the inserted molecules or ions, thus producing a

FIGURE 7.1 The zeolite building units. Two SiO_4/AlO_4 tetrahedra linked by corner sharing.

7.2 FRAMEWORKS

The primary building units of zeolites are $[SiO_4]^{4-}$ and $[AlO_4]^{5-}$ tetrahedra (Chapter 1) linked together by **corner sharing,** forming oxygen bridges (Figure 7.1). The oxygen bridge is not usually linear—the Si/Al—O—Si/Al linkage is very flexible and the angle can vary between 120° and 180°. Silicon-oxygen tetrahedra are electrically neutral when connected together in a three-dimensional network as in quartz, SiO_2 (Figure 7.2). The substitution of Si(IV) by Al(III) in such a structure, however, creates an electrical imbalance, and to preserve overall electrical neutrality, each $[AlO_4]$ tetrahedron needs a balancing positive charge. This is provided by exchangeable cations such as Na^+, held electrostatically within the zeolite.

It is possible for the tetrahedra to link by sharing two, three, or all four corners, thus forming a variety of different structures. The linked tetrahedra are usually illustrated by drawing a straight line to represent the oxygen bridge connecting two tetrahedral units. In this way, the six linked tetrahedra in Figure 7.3(a) and Figure 7.3(b) are simply represented by a hexagon (Figure 7.3(c)). This is known as a **6-ring,** and a tetrahedrally coordinated atom occurs at each intersection between two straight lines. As we see later, many different ring sizes are found in the various zeolite structures.

Many zeolite structures are based on a secondary building unit that consists of 24 silica or alumina tetrahedra linked together; here we find 4- and 6-rings linked together to form a basket-like structure called the **sodalite unit** (also known as the **β-cage**) depicted in Figure 7.4, and which has the shape of a **truncated octahedron** (Figure 7.5). Several of the most important zeolite structures are based on the sodalite unit (Figure 7.6).

The mineral **sodalite** is composed of these units, with each 4-ring shared directly by two β-cages in a primitive array. Note that the **cavity** or **cage** enclosed by the eight sodalite units depicted in Figure 7.6(a) is actually a sodalite unit (i.e., sodalite units are space-filling). In this three-dimensional structure, a tetrahedral Si or Al atom is located at the intersection of four lines because oxygen bridges are made by corner-sharing from all

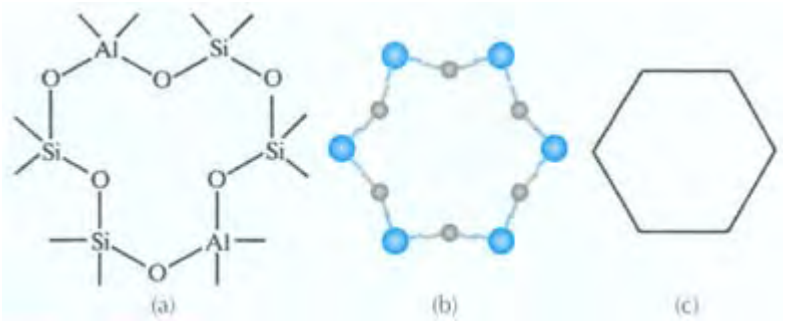

FIGURE 7.3 (a) 6-ring containing two Al and four Si atoms, (b) computer model of the 6-ring, and (c) shorthand version of the same 6-ring.

FIGURE 7.4 The sodalite unit.

shares its octagonal face with six others), forming channels which run parallel to the three cubic axial directions through these large cavities. The computer-drawn models in Figure 7.7 are of the zeolite A framework, illustrating the cavity and its 8-ring window more clearly as well as how it links to a sodalite cage. The formula of zeolite A is given by: $Na_{12}[(SiO_2)_{12}(AlO_2)_{12}].27H_2O$. In this typical example, the Si/Al ratio is unity, and we find that in the crystal structure the Si and Al atoms strictly alternate.

The structure of **faujasite,** a naturally occurring mineral, is illustrated in Figure 7.6(c). The sodalite units are linked by oxygen bridges between four of the eight 6-rings in a tetrahedral array. The tetrahedral array encloses a large cavity (sometimes known as the α-cage) entered through a 12-ring window. The synthetic zeolites

The International Union of Pure and Applied Chemistry (IUPAC) introduced a three-letter structure code to try and simplify matters; zeolite A and the more siliconrich zeolite, ZK-4, have the same framework structure and are designated LTA. Similarly, ZSM-5 and its silicon-rich relation, silicalite, have the same framework and are both designated MFI.

Zeolites are also often written as M-[zeolite], where M refers to the particular cation in the structure (e.g., Ca-zeolite A).

FIGURE 7.7 (a) The zeolite A framework; (b) a sodalite unit in zeolite A, illustrating the linkage to the truncated cuboctahedral cavity.

7.2.3 Si/Al RATIOS

We saw that zeolite A has a Si/Al ratio of 1. Some zeolites have quite high Si/Al ratios: zeolite ZK-4 (LTA), with the same framework structure as zeolite A, has a ratio of 2.5. Many of the new synthetic zeolites that have been developed for catalysis are highly siliceous: **ZSM-5** (MFI) can have a Si/Al ratio which lies between 20 and ∞ (the latter, called silicalite (see Section 7.2.2) being virtually pure SiO_2); this far outstrips the ratio of

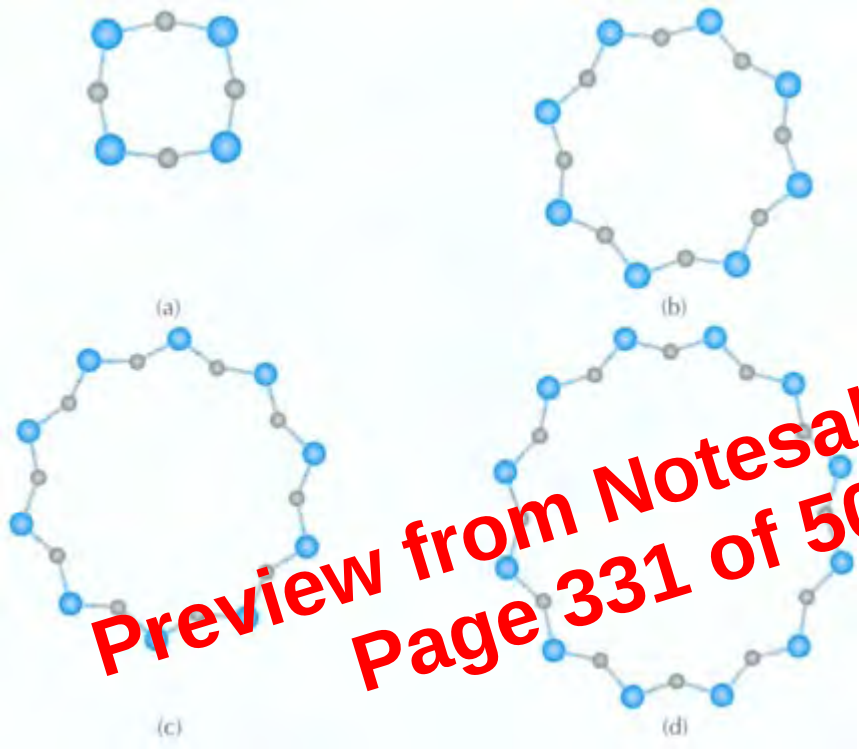

FIGURE 7.9 Computer models of various window sizes in zeolites: (a) 4-ring, (b) 8-ring, (c) 10-ring, and (d) 12-ring.

importance of the number of tetrahedra forming the window (i.e., the ring size). Figure 7.9 illustrates how the window sizes can vary.

The windows to the channels thus form a three-dimensional sieve with mesh widths between about 300 and 1000 pm, thus the well-known name **molecular sieve** for these crystalline aluminosilicates. Zeolites thus have large internal surface areas and high sorption capacities for molecules small enough to pass through the window into the cavities. They can be used to separate mixtures such as straight-chain and branched-chain hydrocarbons.

The zeolites fall into three main categories. The channels may be parallel to: (i) a single direction, so that the crystals are fibrous; (ii) two directions arranged in planes, so that the crystals are lamellar; or (iii) three directions, such as cubic axes, in which strong bonding occurs in three directions. The most symmetrical structures have cubic symmetry. By no means do all zeolites fall neatly into this classification; some, ZSM-11 for instance, have a dominant two-dimensional structure interlinked by smaller channels. A typical fibrous zeolite is edingtonite (EDI), $Ba[(AlO_2)_2(SiO_2)_3].\ 4H_2O$, which has a

aluminium in a zeolite is at its maximum, and the Si and Al atoms alternate throughout this structure.

When it comes to locating the cations, other problems arise. Not every cation site is completely occupied, so although the cation sites can be located, their occupancy is averaged. Furthermore, zeolites are usually microcrystalline and for successful diffraction studies larger single crystals are needed (although Rietveld powder techniques have been successfully applied, especially with neutrons, see Chapter 2). One of the techniques currently being used to elucidate zeolite structures successfully is magic angle spinning NMR spectroscopy (MAS-NMR) (see Chapter 2). Five peaks can be observed for the ^{29}Si spectra of various zeolites, which correspond to the five possible different Si environments. Four oxygen atoms coordinate each Si, but each oxygen can then be attached either to a Si or to an Al atom giving five possibilities:

1. $Si(OAl)_4$
2. $Si(OAl)_3(OSi)$
3. $Si(OAl)_2(OSi)_2$
4. $Si(OAl)(OSi)_3$
5. $Si(OSi)_4$

Characteristic ranges of these shifts are assigned to each coordination type.

Determining the ^{27}Al MAS-NMR spectrum of a zeolite can distinguish three different types of aluminium:

1. Octahedrally coordinated $[Al(H_2O)_6]^{3+}$ trapped as a cation in the pores with a peak at about 0 ppm ($[Al(H_2O)_6]^{3+}$(aq) is used as the reference).
2. Tetrahedral Al, $Al(OSi)_4$, which gives a single resonance with characteristic Al chemical shift values for individual zeolites in the range of 50 to 65 ppm.
3. Tetrahedral $[AlCl_4]^-$, which gives a peak at about 100 ppm; such a peak can occur when a zeolite has been treated with $SiCl_4$ to increase the Si/Al ratio in the framework and should disappear with washing.

An important feature of ^{29}Si MAS-NMR spectra is that measurement of the intensity of the observed peaks allows the Si/Al ratio of the framework of the sample to be calculated. This can be extremely useful when developing new zeolites for catalysis, as much research has concentrated on making highly siliceous varieties by replacing the Al in the framework. Conventional chemical analysis only gives an overall Si/Al ratio, which includes trapped octahedral Al species and $[AlCl_4]^-$, which has not been washed away. At high Si/Al ratios, ^{27}Al MAS-NMR results are more sensitive and accurate and so are preferred.

Even with this information, it is still an extremely complicated procedure to decide where each linkage occurs in the structure. The cation positions can give useful information because they tend to be as close as possible to the negatively charged Al sites.

High resolution electron microscopy (HREM) is also used extensively for structural examination of zeolites, particularly for intergrowths and faults. EXAFS has been used to determine the local coordination geometry of the exchangeable cations and how this changes on reaction or dehydration.

Product Shape-Selective Catalysis

One of the industrial processes using ZSM-5 provides us with an example of product shape-selective catalysis: the production of 1,4-*(para-)*xylene. *Para*-xylene is used in the manufacture of terephthalic acid, the starting material for the production of polyester fibres such as 'Terylene'.

Xylenes are produced in the alkylation of toluene by methanol:

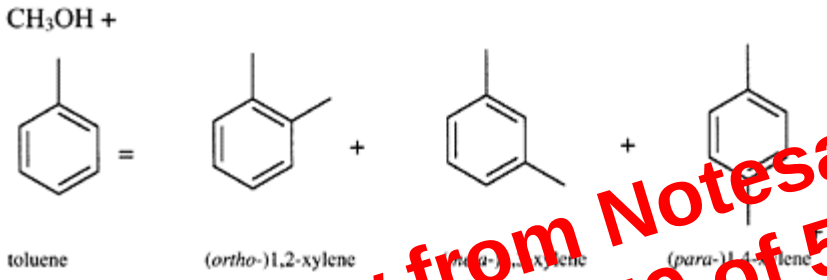

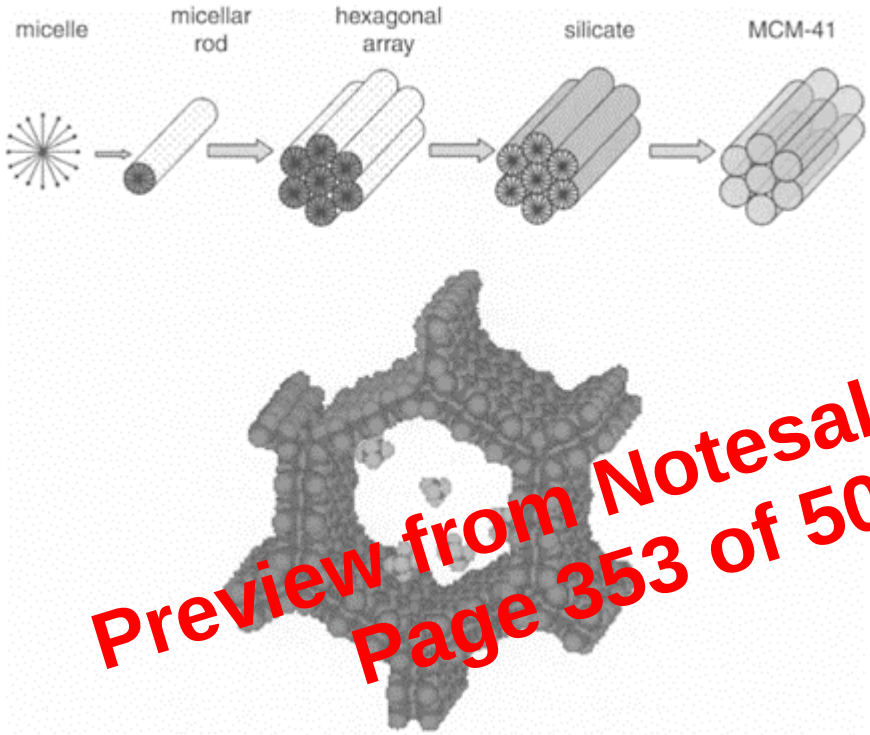

FIGURE 7.21 (a) Possible preparative route for the formation of MCM-41 by liquid crystal templating; (b) computer graphic of ethane and methane molecules inside one of the hexagonal pores of MCM-41. See colour insert following page 356. (Courtesy of Vladimir Gusev, Romania.)

- by direct synthesis;
- by grafting on to the surface using alcohols, silanols, or organosilicon compounds;
- further modification of a functionalized surface by chemical reaction, or by heating.

Organically modified MCM-41 can be prepared directly by using alkoxysilanes or organosiloxanes in the synthesis mixture thus coating the internal wall of the pores with functional groups. An example of a condensation reaction of an alcohol with the surface silanol groups to modify the pore wall is shown in Figure 7.22.

three corners to form an infinite layer. The aluminate layers contain a plane of octahedrally coordinated edge-linked aluminium ions, sandwiched between two inward pointing sheets of corner-linked [SiO_4] tetrahedra. If there is no replacement of Si or Al, then the layers are electrically neutral, producing the mineral pyrophyllite. In the smectite clays, different structures are formed because substitution of silicon and aluminium by metal ions can take place in both the tetrahedral and octahedral layers, the resulting negative charge is distributed on the oxygens of the layer surface, and any charge balance is restored by interlayer cations (usually Na^+ or Ca^{2+}). For instance, in montmorillonite, approximately one-sixth of the Al^{3+} ions have been replaced by Mg^{2+}, whereas in beidellite about one-twelfth of the Si^{4+} have been replaced by Al^{3+}. The different members of the smectite group of clays are distinguished by the type and position of the cations in the framework.

The peculiar layer structure of these clays gives them cation exchange and intercalation properties that can be very useful. Molecules, such as water, and polar organic molecules, such as glycol, can easily intercalate between the layers and cause the clay to swell. Water enters the interlayer region as integral numbers of complete layers. Calcium montmorillonite usually has two layers of water molecules but the sodium form can have one, two, or three water layers; this causes the interlayer spacing to increase stepwise from about 960 pm in the dehydrated clay to 1250, 1550, and 1900 pm as each successive layer of water forms.

The Na^+ and Ca^{2+} cations which make up the charge balance due to the substitution of Si and Al in the layers by other metal ions are strongly hydrated and are located in the interlayer regions, loosely bound to the layer surfaces. They are known as **exchangeable cations,** and can be replaced easily by other cations using ion exchange methods or by protons in the form of H_3O^+, to form an acidic clay. Such acidic clays form very useful catalysts when the reactant molecules enter the interlayer regions. For many years, modified clays were used as the catalyst for petroleum cracking to produce petrol, although they have since been replaced by more thermally stable and selective zeolites. However, smectite clays can be used for the dimerization of oleic acid, the conversion of hexene to dihexyl ethers, and the formation of ethyl

8.2.2 PHOSPHORS IN FLUORESCENT LIGHTS

Phosphors are solids which absorb energy and re-emit it as light. As in the lasers we have just described, the emitter is usually an impurity ion in a host lattice. However, for the uses to which phosphors are put it is not necessary to produce intense, coherent beams of light, and the emitting process is spontaneous instead of induced. Phosphors have many applications, for example, the colours of your television picture are produced by phosphors that are bombarded with electrons from a beam (cathode rays) or from a transistor (flat screen LCD displays). In terms of tonnage produced, one of the most important applications is the fluorescent light tube.

Fluorescent lights produce radiation in the ultraviolet (254 nm) by passing an electric discharge through a low pressure of mercury vapour. The tube is coated inside with a white powder which absorbs the ultraviolet light and emits visible radiation. For a good fluorescent light, the efficiency of the conversion should be high and the emitted light should be such that the appearance of everyday objects viewed by it should resemble as closely as possible their appearance in daylight. Most phosphors for fluorescent lights have been based on alkaline earth halophosphates such as $3Ca_3(PO_4)_2.CaF_2$. As in lasers, the usual dopants are transition metal or lanthanide ions but more than one impurity ion is needed to approximate the whole visible spectrum. For all the impurity ions need to be capable of absorbing the exciting radiation. However, as the host lattice can act to transmit the energy from one site to another. For example, in a phosphor doped with Mn^{2+} and Sb^{3+} ions, the ultraviolet radiation from the mercury lamp is only absorbed by the antimony (Sb^{3+}) ions. The excited antimony ion drops down to a lower excited state via a non-radiative transition. Emission from this lower state produces a broad band in the blue region of the visible spectrum. Some of the energy emitted by the antimony travels through the host crystal and is absorbed by the manganese ions. The excited Mn^{2+} ions emit yellow light and return to the ground state. The two emission bands together produce something close to daylight. Phosphors have been introduced which are more efficient and give a closer approximation to daylight. A good approximation is, for example, given by a combination of blue from barium magnesium aluminate doped with divalent europium (Eu^{2+}), green from an aluminate doped with cerium (Ce^{3+}) and terbium (Tb^{3+}) ions, and red from yttrium oxide doped with trivalent europium (Eu^{3+}).

Fluorescent lights also emit broadband radiation in the near infrared. Finding luminescent materials that will convert this to visible light has generated much interest. In this case, the incident light is of lower energy than the emitted light and the process is known as **upconversion**. Such processes are also exploited in upconversion lasers where a phosphor is used to produce shorter wavelength light from a red laser. Obviously, a ground state atom or ion cannot absorb a photon of one frequency radiation and then emit a photon of higher frequency radiation from the excited state reached by the absorption process. So how does upconversion work?

In upconversion systems absorption takes place in two stages. An ion absorbs a photon of the incident radiation and goes to an excited state. It then transfers most of the energy either to another state of that ion or to the excited state of another ion. If this second excited state is metastable, it has time to absorb another photon before it spontaneously

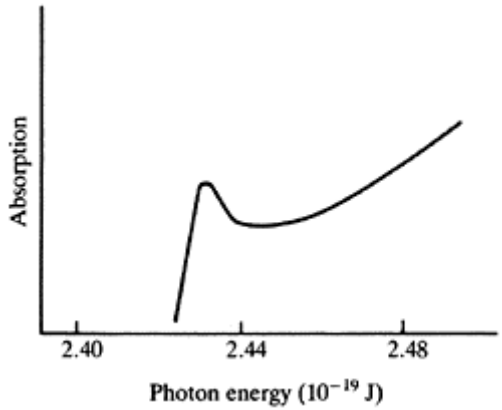

FIGURE 8.7 Absorption spectrum of GaAs.

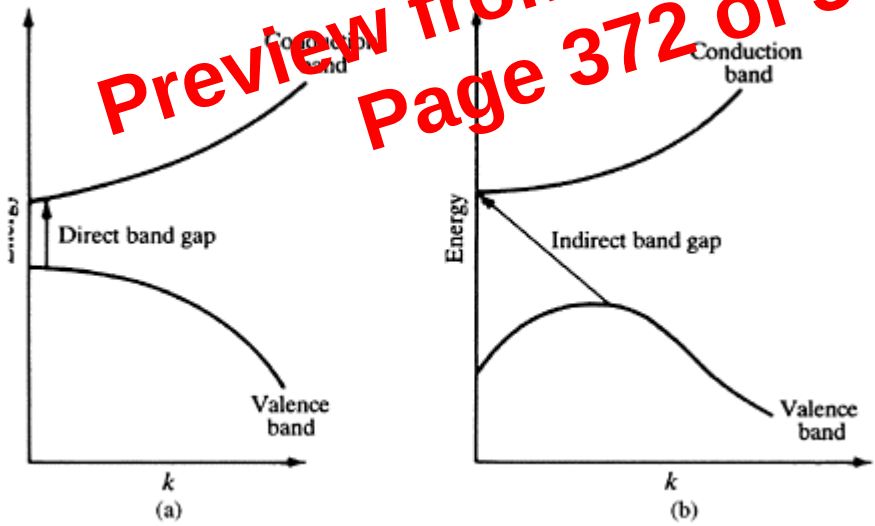

FIGURE 8.8 Sketch of energy bands for (a) a solid with a direct band gap and (b) a solid with an indirect band gap. Note that in this diagram the horizontal axis is *k*, not the density of states. In this representation, a band is depicted as a line going from 0 to the maximum value of *k* occurring for that band.

surface. If the surface is sufficiently regular, then solids which reflect visible radiation appear shiny. Thus, silicon, with a band gap that is at the lower end of the visible region and has allowed transitions covering most of the visible wavelengths, appears shiny and metallic. Many metals have strong transitions between the conduction band and a higher energy band, which lead to their characteristic metallic sheen. Some metals, such as tungsten and zinc, have a band gap in the infrared, and transitions in the visible are not so strong. These metals appear relatively dull. Gold and copper have strong absorption bands due to excitation of d band electrons to the *s/p* conduction band. In these elements, the *d* band is full and lies some distance below the Fermi level (Figure 8.10). The reflectivity peaks in the yellow part of the spectrum and blue and green light are less strongly absorbed, hence the metals appear golden. Very thin films of gold appear

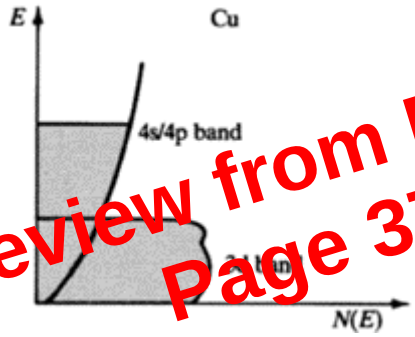

FIGURE 8.10 Band structure of copper.

green because the yellow and red light is absorbed, and only the blue and green transmitted.

Insulators typically have band gaps in the ultraviolet, and unless a localised transition occurs in the visible region of the electromagnetic spectrum, appear colourless.

The devices which we consider involving band gap transitions are, however, concerned with emission of light instead of absorption or reflection; the electrons being initially excited by electrical energy.

8.3.1 LIGHT-EMITTING DIODES

Light-emitting diodes (LEDs) are widely used for displays. Similar to transistors, they are based on the *p*-*n* junction but the voltage applied across the *p*-*n* junction in this case leads to the emission of light.

Figure 8.11 is a *p*-*n* junction in a semiconductor such as GaAs.

The band structure depicted is for the junction in the dark and with no electric field applied. Now suppose that an electrical field is applied so that the *n*-type is made negative relative to the *p*-type (i.e., in the reverse direction to the applied voltage in transistors; see Chapter 4). Electrons will then flow from the *n*-type to the *p*-type. An electron in the conduction band moving to the *p*-type side can drop down into one of the

channel given as a binary code (that is a series of 0s and 1s). This is converted to a series of pits in tracks on the disc spaced approximately 1.6 μm apart. A laser is focused on the disc and reflected on to a photodetector. The pits cause some of the light to be scattered thus reducing the intensity of the reflected beam. The signal read by the photodetector is read as 1 when a high intensity of light is present and as 0 when scattering reduces the intensity. The binary code is thus recovered and can be converted back to sound or pictures. DVDs are similar but use a laser of shorter wavelength which can read more closely spaced pits. This means more information can be packed into a given area.

8.3.3 QUANTUM WELLS—BLUE LASERS

Blue lasers allow higher resolution, and hence higher density of optical storage of information, on devices such as DVDs than the infrared GaAs lasers allow. The earliest blue lasers were based on ZnSe but their lifetime proved too short for commercial applications. Lasers based on gallium nitride (GaN), first demonstrated in 1995, have proved to have greater lifetimes. In these lasers, the photons are produced not in a bulk semiconductor but in quantum wells.

The active region of GaN lasers consists of pure GaN containing several thin layers (30–40 Å thick) of indium doped-GaN, $In_xGa_{1-x}N$. The addition of indium reduces the band gap within the thin layers so that the bottom of the conduction band is at lower energy than that in the bulk GaN. Electrons in this conduction band are effectively trapped because they need to gain energy from an external source to pass into the conduction band of the bulk GaN. Figure 8.13 illustrates schematically the bottom of the conduction band and the top of the valence band for a series of thin layers of $In_xGa_{1-x}N$ in GaN.

The trapped electrons behave like particles in a box (see Chapter 4) but with finite energy walls to the box. Such boxes are **quantum wells**. Within the well, the electron energy is quantised and the spacing of the energy levels depends on the (energy) depth and (spatial) width of the well. The depth of the wells is controlled by the extent of doping (i.e., the value of x). Although the electrons in the wells have insufficient energy to surmount the energy barrier to reach the next well, the probability exists that they will move to a similar energy level in the next well via quantum mechanical tunnelling. Electrons travelling from the bulk GaN enter a high level in the first well (Figure 8.13). From this level, the electron can emit a photon

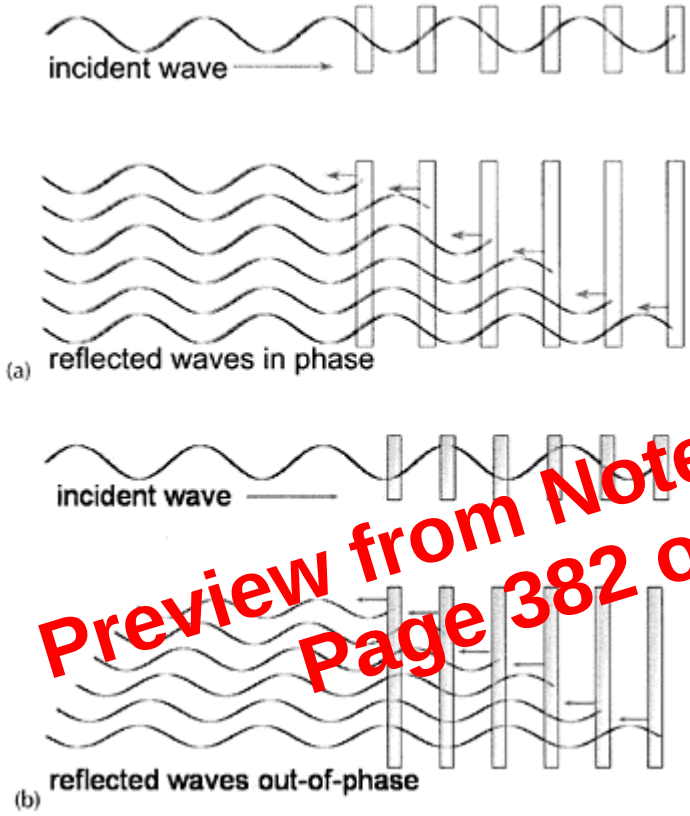

FIGURE 8.15 A row of dielectric slabs. Light travelling through can interfere destructively with reflected light giving rise to forbidden wavelengths. In (a) the reflected waves are all in phase with one another and destructive interference occurs. In (b) the spacing of the slabs is such that the waves are reflected with slightly different phases and the incident light travels through the array.

Two-dimensional photonic materials (i.e., materials in which light is blocked within a plane but transmitted perpendicular to the plane) are useful as optical fibres. An ingenious method of constructing such fibres is to pack a series of hollow capillary tubes around a central glass core. The structure is then heated and drawn until it is only a few μm thick. The central core is now surrounded by a periodic array of tubes of the right diameter to have a photonic band gap in the near infrared. It is also possible to replace the central glass core by air and this enables very high power laser signals to be transmitted along the fibre without damage to the fibre material.

Other potential applications of photonic crystals include crystals with rows of holes to guide radiation around sharp bends (something that cannot be attained with conventional optical fibres), nanoscopic lasers formed from thin films, ultrawhite pigment formed from a regular array of submicron titanium dioxide particles, radiofrequency reflectors for magnetic resonance imaging (MRI) and LEDs.

Photonic crystals have only been studied in the laboratory for two decades, but naturally occurring examples exist, with the best known being the gemstone opal. Opals consist of tiny spheres of silica arranged in a face centred cubic structure. These are thought to have formed from colloidal silica solutions, and the colour depends on the size of the spheres.

QUESTIONS

1. In the oxide MnO, Mn^{2+} ions occupy octahedral holes in an oxide lattice. The degeneracy of the 3*d* levels of manganese are split into two, as for Ti^{3+}. The five *d* electrons of the Mn^{2+} ions occupy separate *d* orbitals and have parallel spins. Explain why the absorption lines due to transitions between the two 3*d* levels are very weak for Mn^{2+}.

2. Figure 8.16 illustrates the energy levels of Nd^{3+} in yttrium aluminium garnet ($Y_3A1_5O_{12}$), which are involved in the laser action of this crystal (known as the neodymium YAG laser). Describe the processes that occur when the laser is working.

3. A phosphor commonly used on television screens is ZnS doped with Cu^{+}. This is much more efficient at transferring energy to the impurity sites for emission than are the phosphors based on phosphates as host. ZnS is a semiconductor. Suggest a reason for the efficiency of transfer in this solid.

4. Figure 8.17 shows two bands for a semiconductor. Is the band gap of this solid direct or indirect?

9
Magnetic and Dielectric Properties

9.1 INTRODUCTION

One consequence of the closeness of atoms in a solid is that properties of the individual atoms or molecules can interact cooperatively to produce effects not found in fluids. A well-known example of this is **ferromagnetism**. In a piece of iron used as a magnet, for example, the magnetism of the iron atoms aligns to produce a strong magnetic effect. Other cooperative magnetic effects lead to a cancelling **(antiferromagnetism)** or partial cancelling **(ferrimagnetism)** of the magnetism of different atoms. Ferro- and ferrimagnets have many commercial applications from compass needles and watch magnets to audio- and videotapes and computer memory devices.

Cooperative effects are not confined to magnetism; similar effects can occur for the response of a crystal to mechanical stress and to electric fields. The electrical analogue of ferromagnetism is the **ferroelectric effect** in which the material develops an overall electrical polarisation, a separation of charge. Ferroelectric materials are important in the electronics industry as capacitors (for storing charge) and transducers (for converting, for example, ultrasound to electrical energy). Ferroelectric crystals are a subclass of piezoelectric crystals and piezoelectric crystals have commercial uses of their own. For example, quartz watches use piezoelectric quartz crystals as oscillators.

This chapter discusses the types of material that display cooperative magnetic and dielectric properties. To begin, however, we consider the weaker magnetic effects that can be found in all types of matter. Then we discuss the origin of the cooperative magnetic effects and their applications. Following magnetic effects we look at dielectric effects, starting with the **piezoelectric effect** and its applications and then considering ferroelectric materials and in particular the oxide barium titanate ($BaTiO_3$), which is widely used as a capacitor.

9.2 MAGNETIC SUSCEPTIBILITY

A magnetic field produces lines of force that penetrate the medium to which the field is applied. These lines of force appear, for example, when you scatter iron filings on a piece of paper covering a bar magnet. The density of these lines of force is known as the **magnetic flux density**. In a vacuum, the magnetic field and the magnetic flux density are related by the permeability of free space, μ_0.

$$B=\mu_0 H \qquad (9.1)$$

as the **remanent magnetisation**. The field that needs to be applied in the reverse direction to reduce the magnetisation to zero is the **coercive force** and is equal to the distance ‘oc’.

9.4.2 PERMANENT MAGNETS

Substances used as permanent magnets need a large coercive force, so that they are not easily demagnetised and preferably should also have a large remanent magnetisation. These substances have fat hysteresis curves. They are often made from

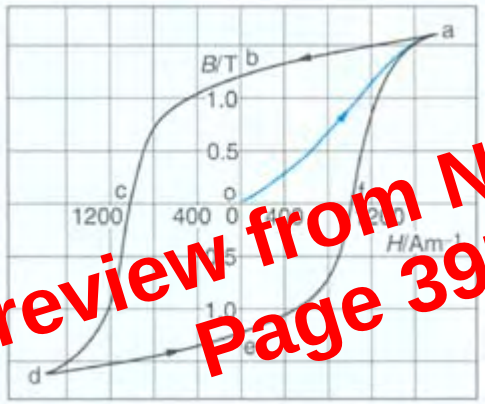

FIGURE 9.7 *B-H* curve for a typical hard steel.

alloys of iron, cobalt, or nickel which form with small crystals and include non-magnetic areas so that domain growth and shrinkage are difficult. Magnets for electronic watches, for example, are made from samarium/cobalt alloys. The best known of these alloys is $SmCo_5$, which has a coercive force of 6×10^5 A m^{-1} compared to 50 A m^{-1} for pure iron.

9.5 FERROMAGNETIC COMPOUNDS—CHROMIUM DIOXIDE

Chromium dioxide (CrO_2) crystallises with a rutile structure and is ferromagnetic with a Curie temperature of 392 K. CrO_2 has metal 3*d* orbitals which can overlap to form a band. In chromium dioxide, however, this band is very narrow and so, similar to Fe, Co, and Ni, chromium dioxide displays ferromagnetism. The dioxides later in the row have localised 3*d* electrons (e.g., MnO_2) and are insulators or semiconductors. TiO_2 has no 3*d* electrons and is an insulator. VO_2 has a different structure at room temperature and it is a semiconductor. It does, however, undergo a phase transition to a metal at 340 K, when it becomes Pauli paramagnetic. Therefore, chromium dioxide occupies a unique position among the dioxides, similar to that of iron, cobalt, and nickel among the first row transition metals, in which dioxides of elements to the left have wide bands of delocalised

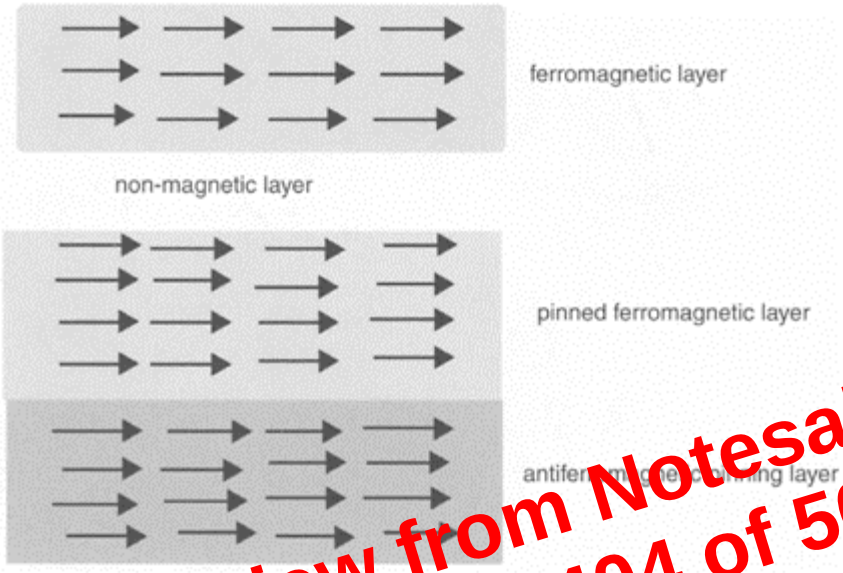

FIGURE 9.13 Two ferromagnetic layers, as in a magnetic hard disk read head, illustrating pinning by an antiferromagnetic layer.

As the read head moves over the hard disk, magnetic fields on the disk cause the spins in the second layer to align either parallel or antiparallel to those in the first layer. The information on the hard disk is coded as a series of 0s and 1s corresponding to the different orientations of the magnetic field on the disk, and these give rise to a high or low current in the read head. GMR read heads can detect weaker fields than earlier read heads, enabling data to be packed more tightly on the hard disk. Their development has led to the high capacity hard disks found in current (2005) laptop computers. A similar principle is used for magnetic random access memory chips (MRAM).

9.8.3 TUNNELLING AND COLOSSAL MAGNETORESISTANCE

A related phenomenon, **tunnelling magnetoresistance (TMR),** has aroused interest as the basis for magnetic sensor and storage devices. Here a thin insulating layer separates the two ferromagnetic layers. Electrons flow from one ferromagnetic layer to the next by quantum mechanical tunnelling.

In 1993, **colossal magnetoresistance (CMR)** was observed for certain compounds such as doped manganite perovskites (e.g., $La_{1-x}Ca_xMnO3$). In these compounds, a change in electrical resistance of orders of magnitude is observed, but large magnetic fields of the order of several tenths of a Tesla (that is a hundred times stronger than those that produce giant magnetoresistance) or larger are needed.

9.10 PIEZOELECTRIC CRYSTALS—α-QUARTZ

A piezoelectric crystal is one that develops an electrical voltage when subject to mechanical stress for example if pressure is applied to it, and conversely develops strain when an electric field is applied across it. Application of an electric field causes a slight movement of atoms in the crystal so that a dipole moment develops in the crystal. For it to be piezoelectric, a crystal must be made up from units that are non-centrosymmetric (i.e., they do not possess a centre of symmetry). Of the 32 crystal classes (see Chapter 1), 11 possess a centre of symmetry and one other cannot be piezoelectric because of other symmetry elements it possesses.

α-quartz is based on SiO_4 tetrahedra. Tetrahedra do not have centres of symmetry and in α-quartz, the tetrahedra are distorted so that each unit has a net dipole moment. However, these tetrahedra are arranged in such a way (Figure 9.15) that normally the crystal does not have an overall polarisation.

External stress changes the Si—O—Si bond angles between tetrahedra so that the dipole moments no longer cancel and the crystal has a net electrical polarisation. The effect in α-quartz is small; the output electrical energy is only 0.01 of the input

FIGURE 9.15 Structure of α-quartz, viewed down a six-fold ring of silicons. Note that the oxygens around each silicon are arranged in a distorted tetrahedron and that the silicons themselves project a distorted hexagon.

strain energy, whereas for Rochelle salt (another commercially used piezoelectric crystal) the ratio of output to input energy is 0.81. α-quartz however is useful in applications

A domain can be of the order of 10^{-5} m or even more. Several methods can be used to obtain pictures of the domains. Figure 9.18 is a photograph taken of a thin slice of barium titanate under a polarising microscope in which different domains can clearly be seen. Note the sharpness of the domain boundaries.

When an external electric field is applied, domains aligned favourably grow at the expense of others. As with ferromagnetics, the response to the field exhibits

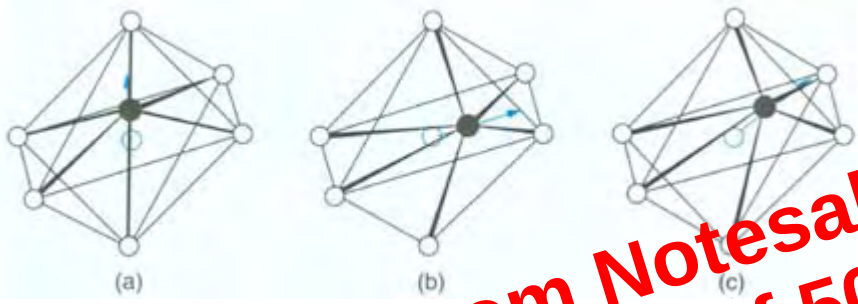

FIGURE 9.16 Distortions of TiO_6 octahedra in (a) the tetragonal structure, (b) the orthorhombic, and (c) the rhombohedral structures of barium titanate.

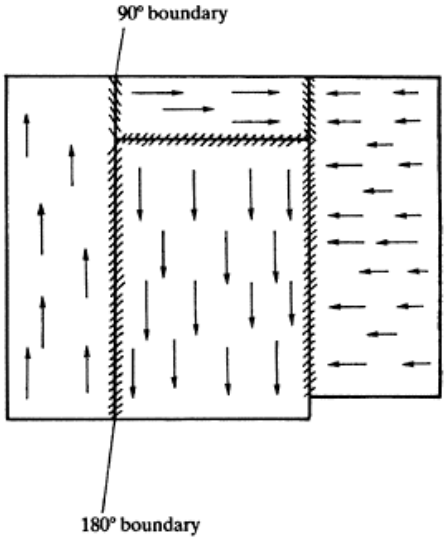

FIGURE 9.17 Sketch of domains in barium titanate, illustrating 90° and 180° boundaries.

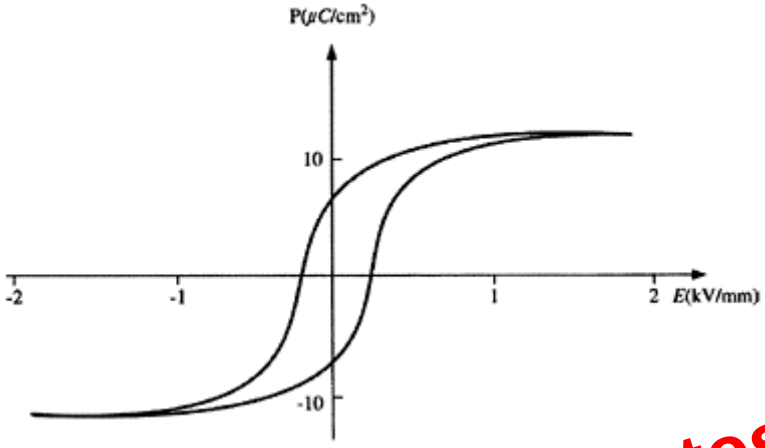

FIGURE 9.19 A plot of polarization vs. applied electrical field for barium titanate of grain size 2×10^{-5}–1×10^{-4} m.

The electric susceptibility and dielectric constant of ferroelectric substances obey a Curie law dependence on temperature (Equation (9.13)).

$$\varepsilon_r=\varepsilon_\infty+C/(T-T_c) \qquad (9.13)$$

where ε_∞ is the permittivity at optical frequencies and T_c is the Curie temperature. The origin of the Curie temperature in barium titanate is quite easy to see because the Curie temperature is the temperature, 393 K, at which barium titanate undergoes a phase transition to a cubic structure. Above the Curie temperature, the structure has a centre of symmetry and no net dipole moment. The dielectric constant is still high because the atoms can be moved off-centre by an applied electric field, but the polarisation is lost as soon as the field is removed.

In $PbZrO_3$, which also has a perovskite structure, the offset atoms are arranged alternately in opposite directions. This produces an antiferroelectric state. $PbZrO_3$ with some zirconium replaced by titanium gives the widely used ferroelectric materials, PZT ($PbZr_{1-x}Ti_xO_3$).

Remarkably some polymers are ferroelectric. Polyvinylene fluoride, $(-CH_2-CF_2-)_n$, as a thin film (approximately 25 μm thick) is used in Shockwave experiments to measure stress. The pressure range over which this polymer operates is an order of magnitude larger than that of quartz or lithium niobate.

In the β-phase of polyvinylene fluoride (PVDF), the CF_2 groups in a polymer chain are all pointing in the same direction (Figure 9.20), so that a dipole moment

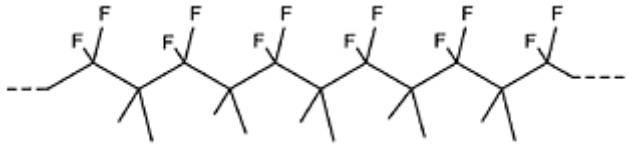

FIGURE 9.20 Alignment of $-CF_2$ groups in β-polyvinylene fluoride.

is produced. Within a domain, the CF_2 groups on different chains are aligned. When an electric field is applied, the chains rotate through 60° increments to align with an adjacent domain.

9.11.1 MULTILAYER CERAMIC CAPACITORS

Capacitors are used to store charge. An electric field is applied to produce charge in the capacitor. The capacitor then remains charged until a current is required. To be useful in modern electronic circuits, including computers, space shuttles, TV sets, and many other applications, a capacitor must be small. In order to retain a high capacitance (i.e., to store a large amount of electrical energy while remaining small), a material needs a high permittivity. Thus barium titanate with its very high permittivity has proved invaluable for this purpose. Pure barium titanate has a high permittivity (about 7000) close to the Curie temperature, but this rapidly drops with temperature to the room temperature value of 1 to 2000. Although this is still high, for electronic circuits it would be useful to retain the higher value so that the size of the capacitor could be reduced. It is also necessary for some applications, for the permittivity to be constant with temperature over a range of 180 K, from 218 K to 398 K. Barium titanate with some of the titanium substituted by zirconium or tin has a Curie temperature nearer room temperature and a flatter permittivity vs. temperature curve. Further improvements can be made by partially substituting the barium ions. Materials made in this way consist of several phases mixed together each with a different Curie temperature, and it is this that gives rise to the flatter permittivity versus temperature curve. Another factor that affects the dielectric properties of barium titanate is the grain size. On the surface of the tetragonal crystals, the structure is cubic, so that for small particles with a large surface to volume ratio there is a high proportion of cubic material. This leads to a higher room temperature permittivity but a smaller Curie temperature permittivity. For very small particles, no ferroelectric effect exists. It is therefore important to produce grains of a suitable size to give the properties needed. To manufacture multilayer capacitors, barium titanate of suitable grain size and appropriately doped is interleaved with conducting plates (Figure 9.21). This enables one device to be used in place of several single disc capacitors in parallel.

delocalised, which band the electrons are in if delocalised, and, in the case of semiconductors, between which two bands the band gap of interest lies.

MnS_2 antiferromagnetic (T_N=78 K), insulator: above T_N paramagnetism fits five unpaired electrons per manganese.

FeS_2 diamagnetic, semiconductor.

CoS_2 ferromagnetic (T_C=115 K), metal.

5. In hydrogen-bonded ferroelectrics, the Curie temperature and permittivity alter when deuterium is substituted for hydrogen. What does this suggest about the origin of the ferroelectric transition in these compounds?

6. Pure $KTaO_3$ has a perovskite structure but is not ferroelectric or antiferroelectric. Replacing some K ions by Li does, however, produce a ferroelectric material. Explain why the substitution of Li might have this effect.

because if the barrier is not too thick then electron pairs can cross the junction from one superconductor to the other without dissociating. This is known as the **d.c. Josephson effect**. He further predicted that the application of a small d.c. electric potential to such a junction would produce a small alternating current—the **a.c. Josephson effect**. These two properties are of great interest to the electronics and computing industries where they can be exploited for fastswitching purposes.

10.2.4 THE BCS THEORY OF SUPERCONDUCTIVITY

This section attempts to give a qualitative picture of the ideas involved and to give some familiarity with the terminology.

Physicists worked for many years to find a theory that explained superconductivity. To begin with, it looked as though the lattice played no part in the superconducting mechanism as X-ray studies demonstrated that there was no change in either the symmetry or the spacing of the lattice when superconductivity occurred. However, in 1950, an **isotope effect** was first observed: for a particular metal, the critical temperature was found to depend on the isotopic mass, M, such that

$$T_C \propto \frac{1}{\sqrt{M}} \tag{10.1}$$

The frequency, ν, of vibration of a diatomic molecule is well known to be given by

$$\nu = \frac{1}{2\pi}\sqrt{\frac{k}{\mu}} \tag{10.2}$$

where μ is the reduced mass of the molecule, and k the force constant of the bond. We can see that a vibration also changes frequency on isotopic substitution such that the frequency, ν, is proportional to $1/\sqrt{\text{mass}}$: this suggested to physicists that superconductivity was in some way related to the vibrational modes of the lattice and not just to the conduction electrons. The vibrational modes of a lattice are quantised, as are the modes of an isolated molecule: the quanta of the lattice vibrations being called **phonons**.

Frohlich suggested that there could be a strong phonon/electron interaction in a superconductor, which leads to an *attractive* force between two electrons that is strong enough to overcome the Coulomb repulsion between them. Very simply, the mechanism works like this: as a conduction electron passes through the lattice, it can disturb some of the positively charged ions from their equilibrium positions, pushing them together and giving a region of increased positive charge density. As these oscillate back and forth, a second electron passing this moving region of increased positive charge density is attracted to it. The net effect is that the two electrons have interacted with one another, using the lattice vibration as an intermediary. Furthermore, the interaction between the electrons is *attractive* because each of the two separate steps involved an attractive Coulomb interaction.

It is the scattering of conduction electrons by the lattice vibrations, phonons, which produces electrical resistance at room temperature. (At low temperatures, it is

also be substituted for the neodymium). Other similar compounds have since been found based on this structure where the three-valent lanthanide is substituted by, for example, four-valent thorium in Nd_{2-x} Th_xCuO_{4-y}. The superconductivity occurs at $T_c \leq 25$ K for these compounds.

It appears clear that these ceramic superconductors all have a common feature—the presence of copper/oxygen layers sandwiched between layers of other elements. The superconductivity takes place in these planes and the other elements present and the spacings between the planes changes the superconducting transition temperature—exactly how is not yet understood

10.3.2 THEORY OF HIGH T_c SUPERCONDUCTORS

The consensus is that, in common with the conventional superconductors, high temperature superconductors contain Cooper pairs (see Section 10.2.4). But a difference occurs in the pairs formed. The Cooper pairs in conventional superconductors couple to give a total angular momentum of zero and are described by an order parameter of *s*-wave symmetry. In high temperature superconductors the Cooper pairs couple to give non-zero angular momentum and are described by an order parameter of *d*-wave symmetry. The pairing state in BCS theory does not need to be caused by electron-phonon interaction, and it is thought that pairing in the *d* state is due to antiferromagnetic spin fluctuations or electron-magnon coupling. Such a possibility had been examined by Kohn and Luttinger, who found that a weak collective residual attraction could be generated from the Coulomb repulsion between electrons, but only if the electrons in the Cooper pairs were prevented from close encounters. This could be achieved if the pairs had angular momentum (i.e., if they were described by *p*- or *d*-waves). Their initial estimate of T_c in such systems was very low, but it was hoped that higher temperatures might be found in metals with strong spin fluctuations. As in BCS theory for conventional superconductors, the coupling is a collective property and the pairing is a dynamic process. Spinmediated coupling is far more effective in bringing about superconductivity in two dimensions than in three and this may explain why high T_c superconductivity is found in quasi-two-dimensional solids such as the cuprates. Experiment suggests that the quasi-two-dimensional organic superconducting polymers (see Chapter 6) are also *d*-wave superconductors.

The presence of *d*-wave symmetry has been demonstrated in an elegant experiment using scanning tunnelling microscopy (STM, see Chapter 2). Collaborators at Berkeley and Tokyo led by J.C.Séamus Davis and Shin-ichi Uchida used STM to measure differential tunnelling conductance on a specimen of bismuth strontium calcium copper oxide with zinc atoms replacing a small number of copper atoms. Differential tunnelling conductance is proportional to the density of states available to electrons tunnelling from the sample into the microscope's tip. This should be zero within a defined energy above the highest occupied levels known as the superconducting symmetry gap. For *d*-wave symmetry, the energy gap is zero in certain directions, resembling the nodes of *d* orbitals. The Zn atoms broke the superconducting pairs at their positions so that a conductance peak appeared at the positions of the Zn atoms. Emanating from the Zn positions were lines of relatively high conductance in the direction of the nodes expected for the *d*-wave function.

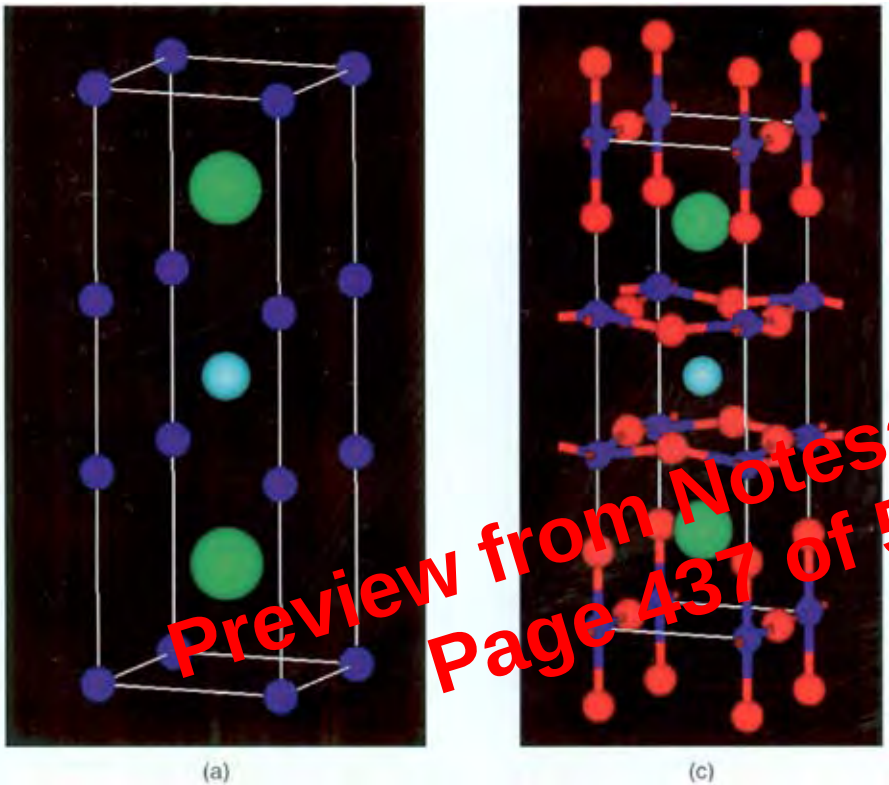

FIGURE 10.8 The structure of 1–2–3: (a) the metal positions; (c) idealized structure of $YBa_2Cu_3O_{7-x}$; (d) the extended structure of $YBa_2Cu_3O_7$, depicting copper-oxygen planes, with the copper-oxygen diamonds in between. Key: Cu, blue; Ba, green; Y, aqua; O, red.

superconductor $Hg_{0.8}Tl_{0.2}Ba_2Ca_2Cu_3O_{8+0.33}$, one fifth of the Hg^{2+} ions are replaced by Tl^{3+} ions and additional oxygen ions are present in the mercury layer. Key: Cu, grey; Ca, red; Ba, blue; Hg/Tl, green; O, aqua.

FIGURE 11.2 The band gap of a semiconductor depends on its size.

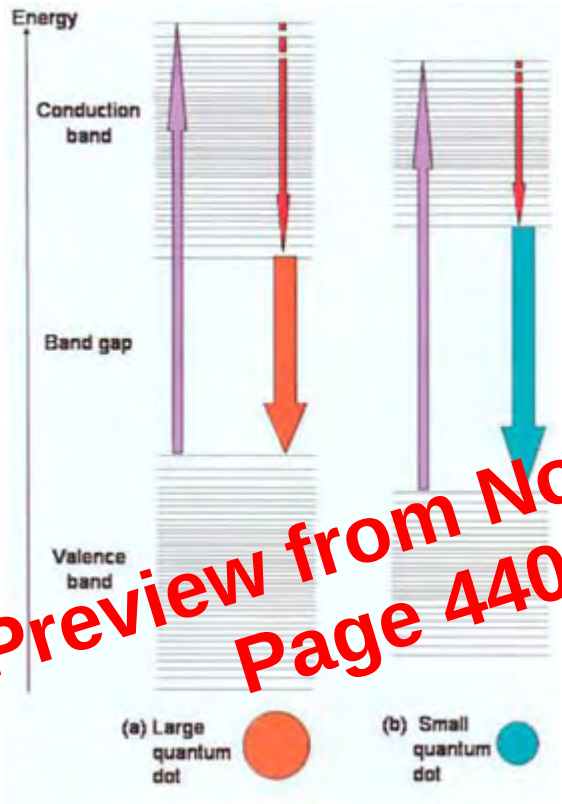

FIGURE 11.7 The colour of the fluorescence from a nano-sized particle depends on its dimensions.

in the newly formed nanocrystal, which would not have the normal thermodynamically stable morphology.

Varying the conditions of deposition of the film in CVD can alter the morphology of the nanocrystals formed; Figure 11.1(a) and Figure 11.1(b) show nanosized diamond crystals in diamond films grown with *111* (octahedral) and *100* (cubic) faces. Techniques for producing specific morphologies could be very important in the production of catalysts because different crystal faces can catalyse very specific reactions.

Many nanomaterials can be made in different forms. We are familiar with the example of carbon, which we can find as diamond films, carbon black, fullerenes, and multi- and single-walled nanotubes. MoS_2 can be made as nanotubes, 'onions' (multi-walled fullerene-type structures), and thin films.

The methods and conditions of nanostructure manufacture are crucial, as we will see that the properties depend critically on the size and shape of particles produced. However, the synthetic techniques used are so particular to each system that they make a subject in their own right and we will not attempt to cover them here.

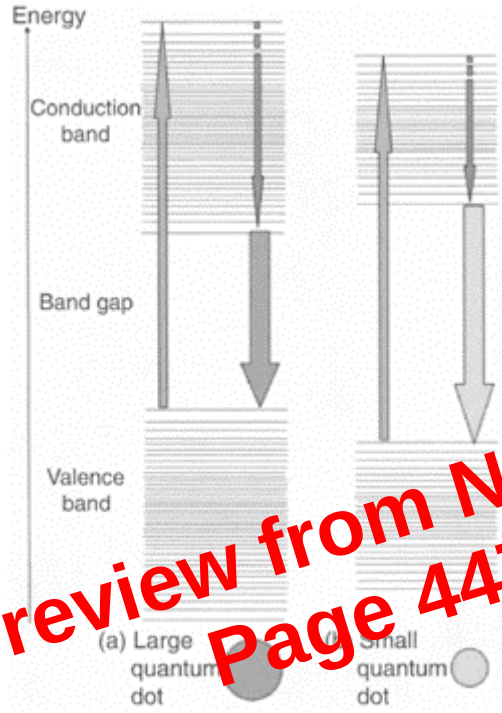

FIGURE 11.7 The colour of the fluorescence from a nano-sized particle depends on its dimensions. See colour insert following page 356.

.

In the absorption spectra of nanoparticles of CdSe and other semiconductors, not only can the shift in wavelength be observed, but there are also bands corresponding to absorption to discrete energy levels in the conduction band. For example, 11.5 nm diameter particles of CdSe have an absorption spectrum that shows an almost featureless edge, but particles of diameter 1.2 nm show features resembling molecular absorption bands shifted about 200 nm to shorter wavelengths, as depicted in Figure 11.8.

The colours produced by nanoparticles of gold (colloidal gold) have been used since Roman times where we find them in the glass of the famous Lycurgus cup (British Museum) which appears green in reflected light and red in transmission. Faraday studied them in detail in the mid-19th century and some of his original samples are still held at the Royal Institution in London. In metals, light interacts with surface electrons and is then reflected. The surface electrons in nanoparticles are induced by the light to oscillate at a particular frequency; absorption at this

layers. In the graphite layer depicted in Figure 11.12, notice that the line joining rows of hexagons in the vertical direction is a simple zigzag, but that at right angles to this, so-called ‘armchair lines’ join the rows. Tubes that roll up along the armchair direction—so-called *armchair* nanotubes—always exhibit metallic levels of conductivity. If graphite sheets roll up along the zigzag lines, with the armchairs along the axis of the tube (*zigzag* nanotubes) or if the sheets roll up along any other

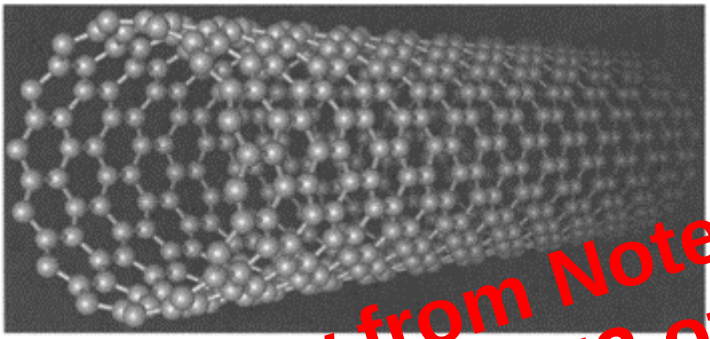

FIGURE 11.11 Computer simulation of a single-walled carbon nanotube.

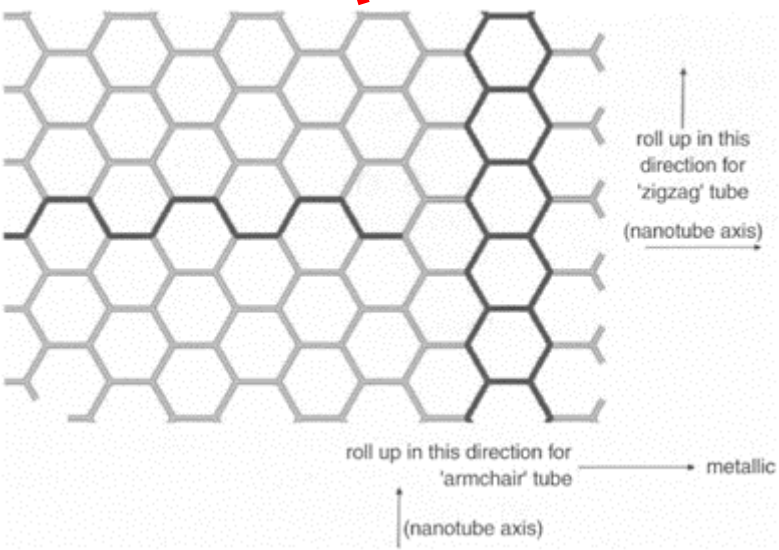

FIGURE 11.12 If the nanosheets roll up in the direction of the arrow, so that the zigzag lines lie along the axis of

the nanotube, then the tubes are usually metallic.

direction except the zigzag or the armchair lines, forming *helical* nanotubes, a band gap is introduced, and the tubes can be semiconducting. It is this property that has allowed the formation of field-effect transistors (FETs), single electron transistors, and diodes from carbon nanotubes. At the time of writing, no preparative method is available for making the type of nanotube needed consistently, they have to be selected by hand from mixtures, but it is hoped that advances will eventually allow the miniaturization of circuitry well beyond that of the silicon chip and ultimately to a molecular computer.

Multiwalled nanotubes have now been synthesized from inorganic compounds; tubes up to 1 μm in length have been formed from WS_2 and MoS_2.

Safety Concerns

Early experiments involving the exposure of mice to nanotubes show that they develop an immune response to them, causing the nanotubes to clump together when inhaled causing lung tissue damage. Both the manufacture and disposal of waste products containing nanotubes will have to be examined carefully.

Nanowires

Nanowires with lengths of several micrometres and diameters of <20 nm have been made from various semiconducting materials, for example, silicon, indium phosphide, and gallium nitride. One method involves creating gold nanoparticles using laser ablation and using these as a catalyst with different gaseous starting materials such as a silicon hydride.

Nanowires can also be deposited from a flowing liquid causing them to lie in the same direction and forming arrays. Changing the direction of flow allows an overlay of a second layer, and such arrays can be used for various electronic devices such as transistors and diodes. The thrust of this type of research is aimed at miniaturization, and ultimately with producing a molecular computer.

11.3.3 THREE-DIMENSIONAL NANOMATERIALS

Nanoparticles

The large surface area of nanoparticles lends increasing dominance to the behaviour of the atoms on the surface of the particle. In catalysis, this is exploited to improve the rate of production in commercial processes, and in the structure of electrodes to improve the performance of batteries and fuel cells (see Chapter 5, Section 5.5.4 and Chapter 7, Section 7.5 and Section 7.6). The interactions between these surface atoms and a surrounding matrix determines the properties of high-performance nanocomposites. Because the dimensions of nanoparticles are less than the wave-length of visible light (400–700 nm), visible light is no longer scattered by them, rendering them transparent; this is a useful property for the manufacture of cosmetics and coatings.

ANSWERS TO CHAPTER 4

1. For the Fermi level in sodium, E=4.5×10^{-19} J and the mass of an electron is 9.11×10^{-31} kg. This gives
4.5×10^{-19}=½×9.11×10^{-31}×v^2

$$v = (2 \times 4.5 \times 10^{-19}/9.11 \times 10^{-31})^{\frac{1}{2}}$$

=9.9×10^5 m s^{-1}

3. (a) N=10^{-12}×(2×9.11×10^{-31}×4.5×10^{-19})$^{3/2}$/3π^2×(1.055×10^{-34})^3
=2.135×10^{16}
(b) 2.135×10^{22}
(c) 0.2
Each level can take two electrons and a crystal of N atoms of sodium has N electrons to fill the band. As you can see, the agreement between the number of filled levels predicted by this very simple theory and the number needed to accommodate the available electrons is very good. Note also that this question illustrates how the energy level spacing increases as the electrons are confined to a smaller and smaller volume.

5. Si, Ge

7. Carborundum like silicon and germanium has 4N valence electrons for a crystal of N atoms. The tetrahedral diamond structure will be favoured because all 4N electrons will then be in bonding orbitals and the energy is lower than in the higher coordination structure.

ANSWERS TO CHAPTER 5

1.

$n_S \approx Ne^{-\Delta H_S/2RT}$ where ΔH_S = 200 kJ mol^{-1} and R = 8.314 J K^{-1} mol^{-1}

TABLE 5.10 Schottky defect concentration in MX compound at various temperatures

Temperature °C	Temperature K	n_s/N	n_s/mol^{-1}
27	300	3.87×10^{-18}	2.33×10^6
227	500	3.57×10^{-11}	2.15×10^{13}
427	700	3.45×10^{-8}	2.08×10^{16}
627	900	1.57×10^{-6}	9.45×10^{17}

3. Increasing the impurity levels does not affect the intrinsic (left-hand side) of the graph. It does, however, increase the value of σ (and thus of Inσ) in the extrinsic region. As the activation energy, E_a, for cation movement stays the same, the slope